UNIVERSITY OF TARTU

Faculty of Science and Technology

Institute of Physics

SEMJON GALAJEV

Degradation processes in $BaMgAl_{10}O_{17}:Eu^{2+}$ and $BaMgAl_{14}O_{23}:Eu^{2+}$

Master's Thesis

Solid-State Physics

Supervisor:

D.Sc. Professor ALEKSANDR LUSHCHIK

Tartu 2008

Contents

Abbreviations

aBR – anti-Beevers–Ross site

AC – alternating current

BAL, $Ba_{0.75}Al_{11}O_{17.25}:Eu^{2+}$ – Barium Aluminate

BAM, $BaMgAl_{10}O_{17}:Eu^{2+}$ – Barium Magnesium Aluminate

BR – Beevers-Ross site

CL – cathodoluminescence

CRT – cathode ray tube

DC – direct current

I – current strength

IR – infrared

mol % – mol percentage

mO – mid-oxygen site

PDP – plasma display panel

PALC – plasma addressed liquid crystal

QY – quantum yield

TSL – thermally stimulated luminescence

TL – thermoluminescence

UV – ultraviolet

U – voltage

VUV – vacuum ultraviolet

TLD(R) – thermoluminescent dosimetry (reader)

1. Introduction

The scientific research on phosphors has a long history starting more than 100 years ago. Why do we need new phosphors? Essentially, because of the technological progress: from the early black and white television, in 1936, to the new 60 in. plasma display panels, the technology has really changed. In the domain of lighting devices - from the first lamp made by Edison to the compact fluorescent lamp used commonly now - progress and improvement are obvious. Research in this field must continue since the excitation sources have changed and it is acknowledged, that a good phosphor for electronic or ultraviolet excitation is not necessarily a good choice for excitation in vacuum ultraviolet (VUV). In a near future, we will be obliged to suppress mercury in any lighting devices because it is very harmful for the environment, and to replace it by a mixture of rare gases - Xenon and Neon. Following blend emits VUV photons from 147 nm to 190 nm instead of ultraviolet photons at $\lambda = 254$ nm that are used to excite the phosphor coated lamp inner surface. Therefore, the fluorescence properties of phosphors induced by such VUV photons have to be studied and improved. In the domain of plasma display panel (PDP) the key factors for success are quality and longevity. Both parameters depend directly on phosphor nature and quality (luminous efficiency, color rendering, durability etc.). Another crucial characteristic of phosphors for PDP is the fluorescence lifetime. The shorter, the better – that is the guideline to produce the highest number of grey levels.

Plasma display panels are a new technique for large-screen television sets and were the object of huge improvements during last decade. Among the various aspects, that need research and development effort, luminous efficacy of spectral transformers has relatively high priority. Their quantum efficiency and stability over a period of time needs to be investigated and improved. In PDP, excitation process is specific due to the nature of VUV, and efficiency and stability are affected mostly by it. Penetration depth of the VUV photons is extremely small, and induces a large involvement of the surface of the phosphor. At first, the luminous efficiency of phosphors decreases during the panel fabrication baking process and thereafter it continues to decrease during the normal operation. This last aging process is very slow (lasts several thousands of hours) and varies from one phosphor to another, inducing a modification of color rendering. Typically, the red component shows a good behavior over time, while the blue and green

components are very sensitive to the aging process. In order to study this process, it is necessary to "accelerate" the time. To do so, it is possible to use a laser, but within the framework of current thesis, a source of X-ray radiation and electron gun were used.

Processes, which may be responsible for aging and are associated with VUV plasma discharge irradiation are: ionic bombardment, surface amorphization, creation of electron–hole pairs, photoionization of doping ions, trapping of energy by impurities. Those, which are relevant to current case, are going to be discussed in detail later. Ageing process is associated with an important decrease in energy transfer efficiency from the host matrices to the emitting centre. It has been proposed [1] that the main reason is essentially the defect density and the formation of traps in the host material. When a VUV photon is absorbed, it creates an electron-hole pair. Then the electron may be trapped by a defect and the energy absorbed is not transferred to the emitting centre. This means that the centre responsible of this absorption band does not transfer its energy to Eu^{2+} ions. The creation of traps associated with VUV excitation has been also confirmed by thermoluminescence experiment. This is one of the reasons why in current research it has been chosen as one of the methods for obtaining experimental data.

General intent of this work is to analyze synthesized Barium Magnesium Aluminate (BAM, $BaMgAl_{10}O_{17}:Eu^{2+}$) and Barium Magnesium Aluminate with different Al_2O_3 and various Eu^{2+} content (that should transform to $BaMgAl_{14}O_{23}:Eu^{2+}$) and to analyze its physical properties. Second goal is to see how various types of radiation influence synthesized compound. This will be done by exposing objects of interest to various doses and types of radiation.

Main subjects of this thesis are:

1. Principle of PDP operation;
2. Overview of blue and red phosphors currently used in PDP, their luminous efficiency, compatibility with other phosphors and radiation stability;
3. Reasoning on prognosis of improved properties;
4. Chosen research methods;
5. Synthesis process of new phosphor for PDP application;
6. Analysis of synthesized compound.

2. Principle of PDP operation

2.1 Structure of plasma display panels

The most popular plasma display panel technology is the one that utilizes micro discharges to generate the light of the display. Second one is the plasma addressed liquid crystal (PALC) technology, where micro discharges serve as electrical switches. Overview of PDP-type technology is going to be given in this work.

The basic idea of a plasma display is to illuminate tiny amounts of different phosphors to form an image. Each pixel on such screen is made up of three fluorescent lights – a red light, a green light and a blue light. Just like a CRT (cathode ray tube), the plasma display varies the intensities of the different lights to produce a full range of colors.

A plasma display panel consists of two glass plates placed at a distance of 100-200 μm from each other. The region between the plates is filled with a gas at a pressure of 0.5-0.6 atmosphere. The plates are covered on the inner side with a large number of thin parallel electrodes, in such a way that the electrodes of one plate are placed perpendicular to the electrodes of the other plate. Therefore, they form rows and columns of a display. At each intersection between a row and a column electrode, a discharge can be formed, independent of the other intersections, by applying suitable voltage pulses to the electrodes. The discharge gives rise to plasma that emits visible and vacuum ultraviolet light. In monochrome PDP the visible light can be used directly. In color PDP, the VUV light is used to excite phosphors, which then emit red, green or blue light [2]. Gases confined between two glass panels are usually mixtures of He-Xe or Ne-Xe. Emitted VUV light typically is peaking at 147 and 173 nm. One of the drawbacks is that the efficiency of the discharge, that will produce VUV radiation, is still quite low and on average is only 10% [3,4].

The discharge can be operated in direct current (DC) or alternating current (AC) mode. In the first case, the electrodes are in direct contact with the discharge gas, whereas in the second case the PDP is covered with a dielectric layer. AC type of discharge has become a mainstream because of simpler structure and longer lifetime. Mainly, coplanar electrode type is used. **Fig. 1** represents a simple scheme of PDP including picture element (i.e. “pixel”) structure. Pixel is formed by the intersection of one pair of sustaining electrodes and one initiating electrode.

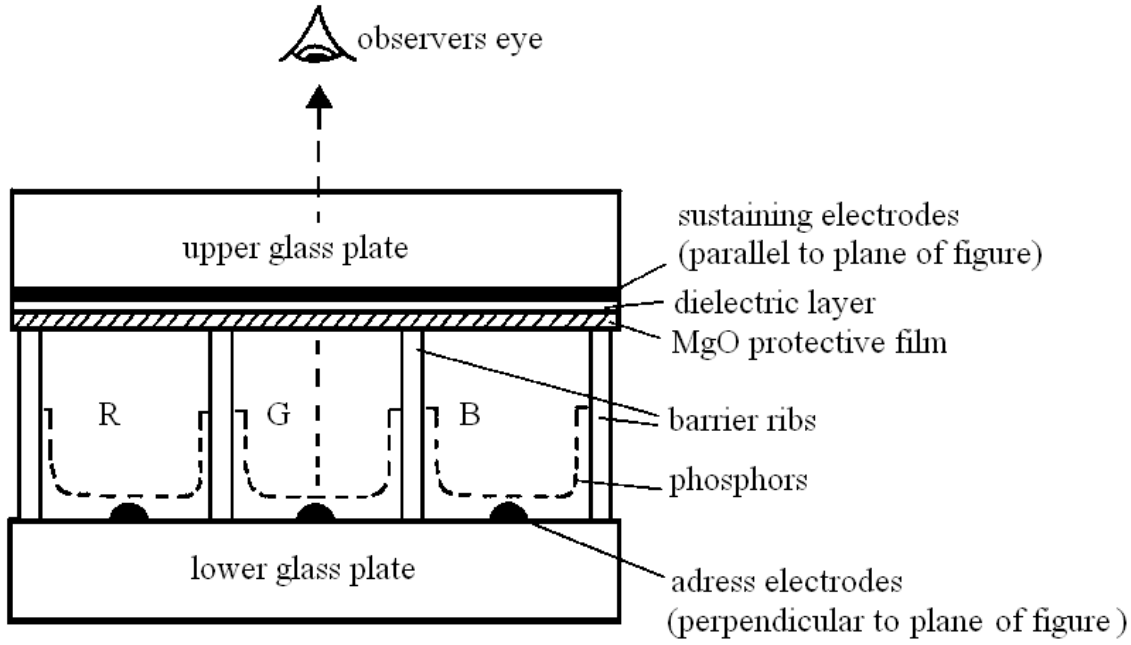

Figure 1. Schematic profile of an a.c. PDP [6].

The discharge is sustained between two pairs of electrodes at the upper plate (sustaining electrodes), whereas the electrodes at the lower plate (address electrodes) are used to ignite the discharge (surface discharge PDP). The electrodes of the upper plate made transparent and covered with a thin glass layer, which serves also as the dielectric. To expand lifetime of PDP, an MgO thin film is deposited to protect against the bombarding ion flux and to enhance secondary electron emission at the surface as well. Dielectric barrier ribs are placed between the initiating electrodes at the lower plate, to prevent electrical and optical interactions between the columns. The lower plate is also covered with consecutive phosphor columns, alternating in red, green and blue [5,6].

Also it must be mentioned, that the overall efficiency of the photon conversion process (including scattering and absorption of the emitted photons) depends on the size of the phosphor particles. Simulations of the photon conversion process in a PDP cell, based on Mie scattering theory, showed, that for a given phosphor layer thickness should be between 20 and 30 μm and optimum diameter of the phosphor particles should be 1-2μm [5,6].

2.2 Performance and luminous efficiency of PDP

Compared to early PDP, which were made in 1990s, modern PDP have now achieved a high level of performance. In the early 1990s, first color plasma displays had very low luminous efficacy (less than 1 lumen per Watt [lm W^{-1}]) and very low contrast. Nowadays, PDP manufacturers report 1-2 lm W^{-1} efficiency for commercially available PDP and 2-3 lm W^{-1} for laboratory samples. The reported luminance is between 500 and 700 cd m^{-2} for 42-63 inch PDP and the announced contrast ratios are 3000:1 in dark viewing conditions and 120:1 in bright light conditions. The reported lifetime can reach 30 000 h. Given information differs from manufacturer to manufacturer, because performance measurements are not yet standardized. Relying on this data, it appears that an important research effort is still needed to improve the luminous efficiency which still remains low compared to CRT (characteristics of CRT are approximately three times higher). To achieve comparable parameters, different ways of improvement are offered: more complex electrode shapes, optimization of cell geometry and gas mixture, material research (both protective and emissive layer, phosphors) and optimization of addressing and sustaining schemes. In spite of the relatively large lifetime announced, it seems that lifetime is still an issue. The initial brightness of a PDP is high (more than 500 cd m^{-2}), but the display quickly loses brightness over time. This is due to the degradation of activated phosphors. The most vulnerable phosphor is the blue light emitting one. According to experiments, conducted by various laboratories, the decrease of the luminance of a PDP can be as large as 10% in 5000 hours in normal operating conditions. The lifetime of the panel corresponds to a 50% decay of the luminance. The overall lifetime of a PDP also depends on the lifetime of the protective and emissive MgO layer. Another remaining issue concerning panel performance is related to image quality [2-6].

The energy balance of a typical PDP discharge is represented in **Table 1** [2]. One of the main energy losses in a PDP discharge is due to ion heating. About 60% of the total electric energy dissipated in a PDP cell is spent in ion heating in the cathode sheath. In that sheath, ion heating is important because of the large ion current and large electric field in this region. From the 40% remaining energy dissipated by electrons. Estimated, that about 50% (that is 20% of the total input energy) is used to excite xenon atoms (the other 50% are spent into electron impact ionization of xenon and neon, and into electron impact excitation of neon).

Energy	%	Loss
dissipated in discharge	**100%**	
	↓	60 % in ion heating
electron heating	$\rho = 40\%$	
	↓	50% in Xe ionization, Ne excitation and ionization
xenon excitation	$\eta_{Xe} = 20\%$	
	↓	25% transition loss
UV production	$\eta_{UV} = 15\%$	
	↓	50 % VUV photons not collected by phosphors
UV energy reaching the phosphors	7.5%	
	↓	67% UV to visible photon energy conversion loss
Visible photons production	2.5%	
	↓	40 % visible photons not collected on front face
Photons reaching the user	**1.5%**	

Table 1. Energy balance in a PDP picture element [2].

Only 20% of the total energy dissipated in the discharge is put into xenon excitation. The xenon system is rather efficient and a large part of the energy put into xenon excitation leads to UV photon emission (about 25% of the energy put into xenon excitation is lost in transitions from upper excited states of xenon to UV emission states). Following **Table 1**, we find that about 15% of the total energy dissipated in the discharge is converted into UV photon energy. Due to the geometry of the cell (phosphors are deposited between the dielectric barrier ribs on the back plate), a large part of the photons is lost, and only around 50% can reach the phosphor layers (carrying 7.5% of the total energy dissipated in the discharge). Even if we assume that each UV photon is converted into a visible photon by the phosphors, the UV-visible conversion is not efficient, because energy difference between the xenon VUV photons and the visible photons is about three times. Following

current estimation, it can be seen, that the visible photons emitted by the phosphors carry about 2.5% of the total energy. Assuming that approximately 40% of the photons are lost and not collected by viewer's eye, this leads to a total efficiency of about 1.5% of the total energy dissipated in the discharge. This, according to rough approximation, corresponds to the luminous efficacy of only 1 to 3 lm W^{-1} of the present PDP [2,4,5].

3. Phosphors and luminescence.

Most phosphors are generally solid inorganic materials whose host lattice is intentionally doped with impurities (see **Fig. 2**). The impurity concentration is generally low, in view of a fact, that at higher concentration the efficiency of the luminescence process usually decreases (so called concentration quenching). Most of the phosphors have a white body color, especially for fluorescent lamps (this is an essential feature to prevent absorption of visible light by the phosphors used). The absorption of energy, which is used to excite the luminescence, takes place by either the host lattice or by intentionally doped impurities. In most cases, the emission takes place on the impurity ions, which are also called activator ions when they generate the desired emission. When absorption of the activator ions is weak, a second kind of impurities can be added (sensitizers). Sensitizers absorb the energy and subsequently transfer it to the activators. This process involves transport of energy through the luminescent materials. Quite frequently, the emission color can be adjusted by choosing the right impurity ion and without changing the host lattice in which they are incorporated. Several activator ions show emission spectra at spectral positions that are hardly influenced by their chemical environment. This is especially true for many of the rare-earth ions [7].

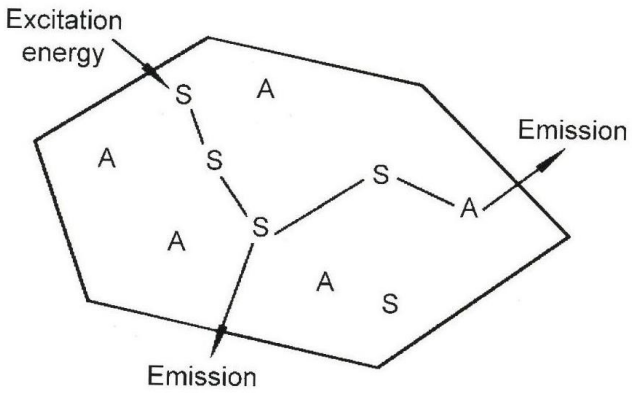

Figure 2. Luminescent material containing activator ions A (ions showing the desired emission) and sensitizing ions S (on which UV excitation can take place) [7].

There are several types of luminescence: center luminescence, charge transfer luminescence, donor-acceptor pair luminescence. In our case, we deal with center luminescence. The emission is generated on an optical center, in contradiction to emission, which results from optical transitions (occurs between host lattice band states or from a transition between two centers). An optical center can be an ion or a molecular ion complex. Characteristic luminescence can consist of relatively sharp emission bands (spectral width typically in a range of few nm), but also of broad bands, which can have widths exceeding 50 nm in the visible part of the spectrum. Broad emission bands are observed when the character of the chemical bonding in the ground and excited state differs considerably. A change in equilibrium distance between the emitting ion and its immediate chemical environment takes place. Usually this process can be explained with the configuration coordinate diagram (**Fig. 3**) [7,8,9].

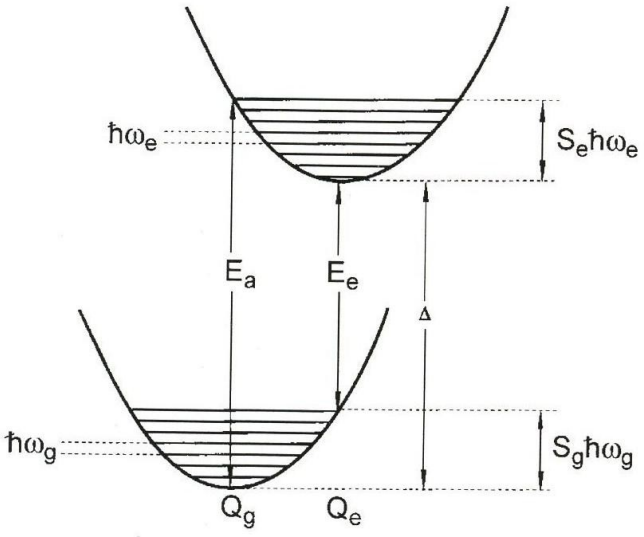

Figure 3. Configurational coordinate diagram [7].

In this diagram, Q_g and Q_e represent the metal-to-ligand distances in the ground and excited states, respectively. E_a and E_e are the energies at which the absorption and emission bands have their maximum intensity, respectively. Δ is the energy of the so-called zero-phonon line; this transition involves completely relaxed excited and ground states, no excited phonon states are involved – hence the name of this kind of transitions. The phonon frequencies in the ground and excited state are given by $\hbar\omega_g$ and $\hbar\omega_e$, respectively. The relaxation energies in the ground and excited states can be expressed as

a product of the phonon energy and the so-called Huang-Rhys factors. The Huang-Rhys factors S_e and S_g in the ground and excited state (being pure numbers), respectively, give the mean number of phonons involved in the absorption and emission processes. This diagram is obvious, but still a simplified model – for example, it does not describe thermal expansion of the lattice (even though, such illustration can be used to show that a larger Stokes Shift is expected on increasing lattice relaxation and also in the description of thermal quenching of the emission) [7,9,10].

For instance, $BaMgAl_{10}O_{17}:Eu^{2+}$ shows efficient blue Eu^{2+} emission; this emission is responsible for the shoulder at 450 nm and often used as blue emitting phosphor in high-quality fluorescent lamps and plasma display panels. The emission descends from the optically allowed 5d-4f transition on Eu^{2+}, which is hence very fast – with a decay time about 1 μs. An example of emission spectrum for $Ba_{0.9}MgAl_{10}O_{17}:Eu^{2+}_{0.1}$ phosphor is presented in **Fig. 4** Emitted photons had maximum energy at 2.73 eV; this matches to a wavelength of 450 nm, which lies in the range of the blue light. Excitation is due to 8.43 eV photons (147 nm), which corresponds to discharge of He-Xe and Ne-Xe gas mixtures.

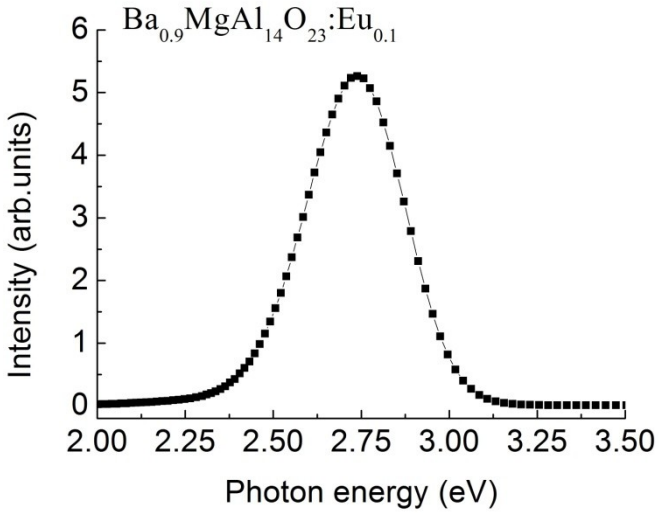

Figure 4. Emission spectrum for $Ba_{0.9}MgAl_{10}O_{17}:Eu^{2+}_{0.1}$ (sample 68(B)). Obtained by colleagues from the Institute of Physics, using synchrotron radiation at HASYLAB at DESY, Hamburg.

Width and position of the emission bands originating from optical transitions within the f-electronic shell are almost independent of the chemical environment. The relative intensity of the separate bands, however, depends on the crystal lattice. The transitions on

many rare-earth ions are spin and parity forbidden and therefore rather slow (in the ms range). However, for a number of rare-earth ions as well as Eu^{2+} ($4f^7$-configuration), due to d → f transition, broadband emission is also possible.

Broad bands are observed for many optical transitions in the partly filled d-shell of transition metal ions (d → d transitions), but also for transitions between the 5d shell and the 4f shell of rare-earth ions (d → f transitions). Sharp emission bands are characteristic of optical transitions between electronic states with chemical bonding character (almost the same for ground and excited state), and for the same reason, optical transitions between electronic states that hardly participate in the chemical bonding (f → f transitions on rare-earth ions). Further in the text, term symbols also are going to be used to describe electronic transitions which arise from the site symmetry of the ions of interest [7,9,11].

3.1 Optical excitation of luminescence

In cases, when absorption of UV or visible light leads to emission of photons – we deal with optical excitation of luminescence. This process takes place in fluorescent lamps, new phosphor-converted LEDs and plasma display panels. Optical absorption can take place on the already discussed impurities (optical centers), being either the activator ions or the sensitizer ions. Sensitizer ions are used when the optical absorption of the activator ions is too weak (e.g., because the optical transition is forbidden) to be useful in practical devices [7]. Nevertheless, this is not that relevant to the case discussed in this thesis. Optical absorption leading to emission can also take place by the host lattice itself – so called band absorption or host lattice sensitization. Energy transfer from host lattice states to the activator ions, and in some cases involving sensitizers, has to take place [8].

In the blue emitting luminescent material $BaMgAl_{10}O_{17}:Eu^{2+}$, both the absorption and the emission processes originate from optical transitions between the 4f and 5d levels of the Eu^{2+} ion. When transition leading to optical absorption is allowed, a relatively small Eu^{2+} concentration (5% to 10% of the Ba^{2+} ions are replaced by Eu^{2+} ions) is sufficient to adjust a satisfactorily strong absorption in practical devices [5,10]. The excitation spectrum of $BaMgAl_{10}O_{17}:Eu^{2+}$ is given in **Fig. 5**.

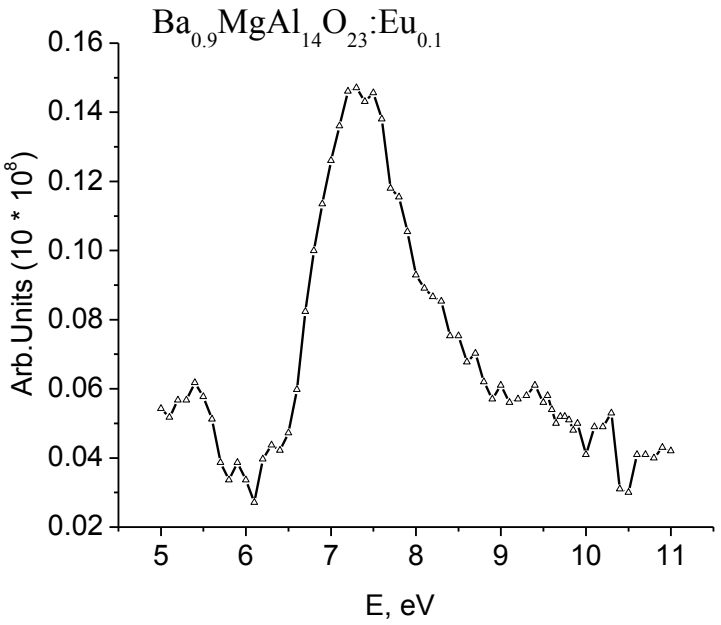

Figure 5. Excitation spectrum for Eu^{2+}-emission measured for a fresh $Ba_{0,9}MgAl_{14}O_{23}:Eu_{0,1}$ sample synthesized in the Institute of Physics. (Vacuum monochromator VMR-2; optical filter С3С-22; T = 300 K, ФЭУ39 (U = 900 V)).

We observe a strong broad absorption spectrum in the VUV part of the range. It must be noted, that the absorption extends into the near UV/blue part of the optical spectrum (not present in **Fig. 5**), and this interesting parameter have been already experimented with. Blue emitting $BaMgAl_{10}O_{17}$: Eu^{2+} with a blue body color (intrinsic pigmentation Co^{2+}) has been synthesized [12]. It yields a phosphor with an improved color point due to the self-absorption of the low-energy tail of the 4f–5d emission band of Eu^{2+}.

Eu^{2+} ions have a $4f^7$ configuration with $^8S_{7/2}$ as ground state. The lowest excited state in the $4f^7$ configuration is $^6P_{7/2}$. The spin and parity for the $^6P_{7/2} \rightarrow {}^8S_{7/2}$ transition are forbidden. Hence, the probability of this transition is low. The next excited state of Eu^{2+} is $4f^65d^1$, which generally lies above the $^6P_{7/2}$ state. The 4f electrons are shielded from the surrounding lattice by 5s and 5p electrons and thus are affected only weakly by changes in the environment. However, the 5d levels are strongly influenced by the crystal field. The $4f^65d^1$ state splits into $4f^65d^1$ (t_{2g}) and $4f^65d^1$ (e_g) levels with the $4f^65d^1$ (t_{2g}) being the lowest [13,14]. The separation between these levels depends on the strength of the crystal field. **Fig. 6** displays schematic energy level diagram as a function of crystal field and plain energy level diagram of Eu^{2+} ion. The energy axis (in eV) is representative for ions in oxidic lattices.

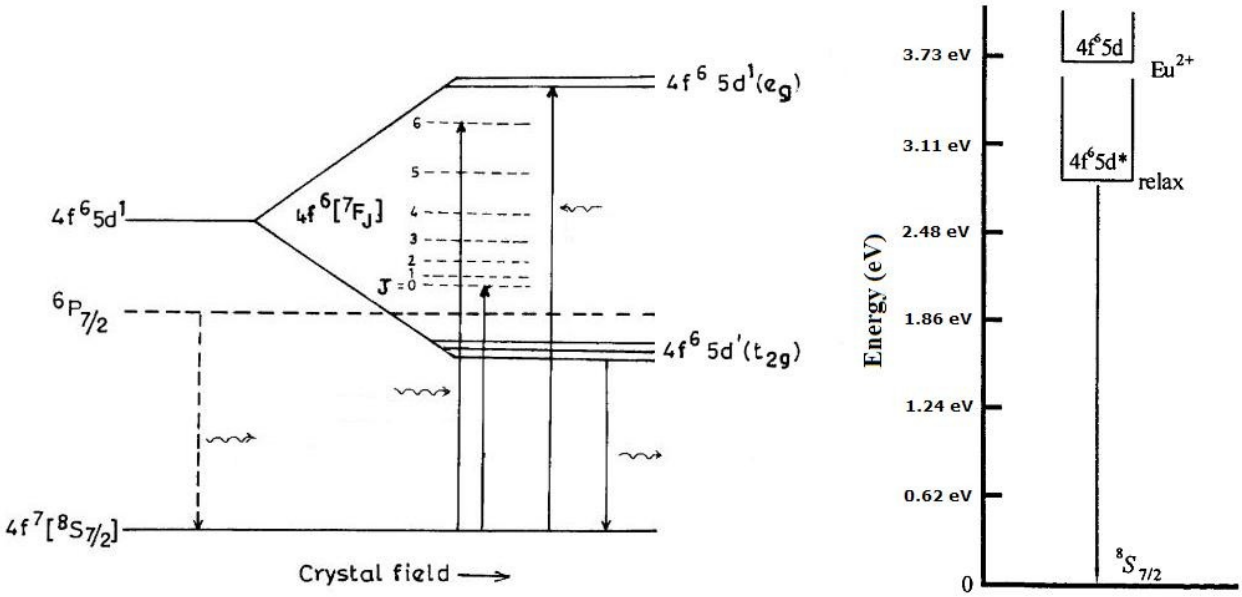

Figure 6. Schematic energy level diagram of Eu^{2+} ion as a functions of crystal field. [13,15].

Usually the emission and absorption spectra consist of broad bands due to transitions between the $^8S_{7/2}$ state and crystal field components of the $4f^6 5d$ configuration. If the lowest $4f^6 5d$ component is situated above the ^6P_J states of the $4f^7$ configuration (crystal field splitting is small), then narrow line emission is observed. This condition can be met in the case of $BaMgAl_{10}O_{17}:Eu^{2+}$, because we substitute larger Ba^{2+} with Eu^{2+}. Another possibility is if Eu^{2+} ion is situated in a lattice with octahedral six-coordination [7,13,14,15].

Fig. 7 demonstrates configuration coordinate diagram for the Eu^{2+} ion. The $^8S_{7/2}$ and $^6P_{7/2}$ state from the $4f^7$ configuration have been drawn. For the lowest-lying crystal-field component two possibilities have been drawn – d and d'. They have in common that the absorption transition from the $^8S_{7/2}$ ground state to these levels is at the same energy (the distance AB in the figure) [16].

Absorption into curve d is finally followed by emission from C (at least at low enough temperatures, since C lies lower than D, the lowest state of curve d). Emission from C (CA in the figure) is a narrow line emission. Absorption into d' is finally followed by emission from E, since E is lower than C. As for emission from E (EF in the figure) – this is broadband emission.

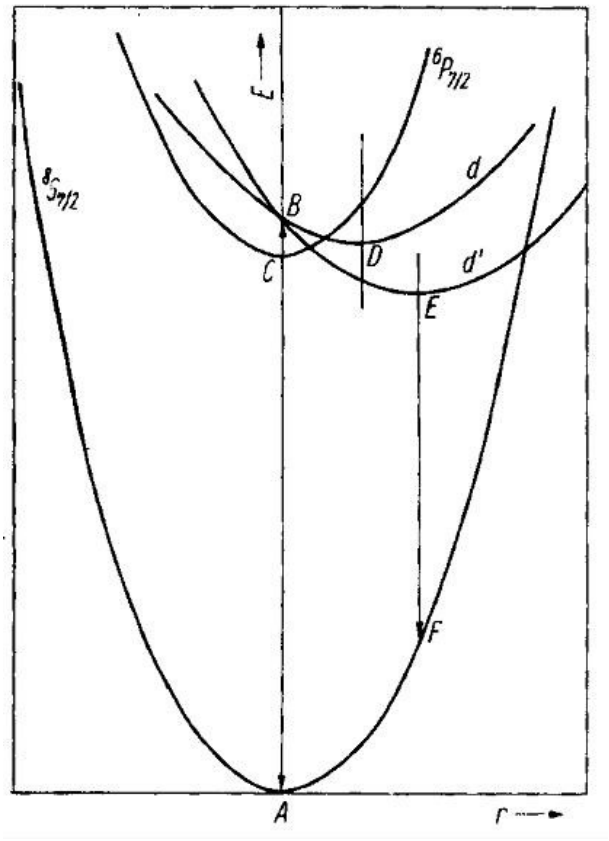

Figure 7. Configuration coordinate diagram of Eu^{2+} [16].

It is clear that the condition for narrow line emission is not only B higher than C, but also C below D (or E). This will be the case, if B is situated above C and if the difference between the equilibrium distances of the $^8S_{7/2}$ ground state and the $4f^6 5d$ state is small (like in curve d). This condition has been translated into the following structural conditions: the cations, neighbors of the Eu^{2+} ion, should be small and have a high charge and the Eu^{2+} ions should be substituted for larger divalent cations [15,16].

3.2 Emission color of BAM

Many luminescent ions show emission at different wavelengths in different host lattices. This phenomenon, once understood, opens up the possibility to change (within certain limits) the emission color. In this way, the emission spectra (and excitation spectra) can be tuned toward the specifications required.

In cases where at least one of the electronic states is involved in the chemical bonding, the coupling to the lattice has to be taken into account. This situation is encountered for many transition metal ions and for rare-earth ions showing d → f emission. As was mentioned before, the electronic configuration of Eu^{2+} is $4f^7$. The lowest excited state of 4f levels is located at about 3.48 eV and is higher than the $4f^6 5d^1$ level in most crystals, so that Eu^{2+} usually gives broadband emission due to f-d transitions. The wavelength positions of the emission bands depend very much on hosts, changing from the near UV to the red. Such dependence usually being interpreted as due to the crystal field splitting of the 5d level. This situation is illustrated for d → f optical transition on Eu^{2+} in **Fig. 8** [7,10,13,15].

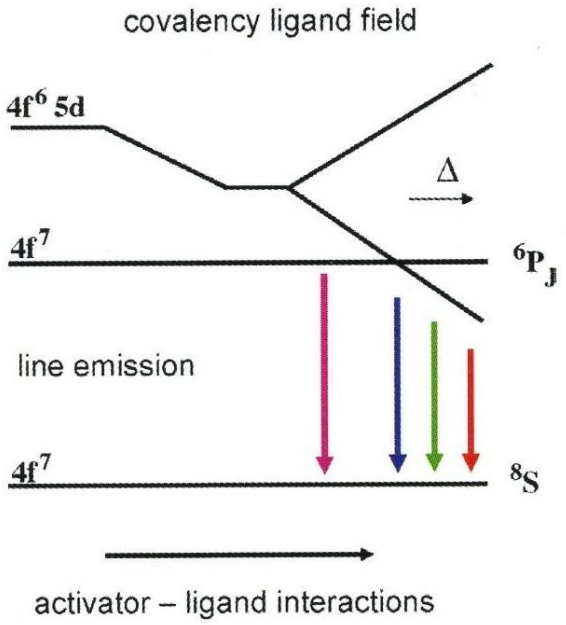

Figure 8. Energy separation of the $4f^7$ and $4f^6 5d^1$ bands in Eu^{2+} as a function of covalence and ligand field strength (Δ - crystal field). The arrows indicate different emission colors – from UV to red. [7, 10]

The energy difference between the d- and f-electrons is modified by the covalence of the Eu^{2+}-ligand bond and the crystal field strength. An increase of the covalence of the Eu^{2+}-ligand bond results in a lower energy difference of the 4f-5d energy separation (due to the nephelauxetic effect) [17]. With increasing crystal field strength, the emission bands shift to longer wavelength. The crystal filed interaction splits the d-level, depending on symmetry and crystal field strength, and for Eu^{2+}, emission from the UV part to the red part can be obtained.

As was mentioned before, even line emission is possible. Sharp-line luminescence at ~ 360 nm due to an f-f transition and having a lifetime of milliseconds is observed when the crystal field is weak, so that the lowest excited state of $4f^7(^6P_J)$ is lower than the $4f^65d^1$ state, as illustrated in **Fig. 8** Both are easily accessible by choosing appropriate host lattices, and for this reason broad-band emitters can in general be tuned within a large spectral range and can be adapted to the application needs.

Also, guided by **Fig. 8** it is possible to explain the lifetime of the Eu^{2+} luminescence, which is still relatively long (10^{-5}-10^{-6} s) for an allowed transition. The ground state of $4f^7$ is ^8S, and the multiplicity of the excited state $4f^65d^1$ is 6 or 8; the sextet portion of the excited state contributes to the spin-forbidden character of the transition.

As for the spectral position of the emission lines, which arise due to transitions between f-electronic states – it does not vary very much on changing the host lattice. However, the relative emission intensity of the several possible optical transitions does vary considerably.

As it was mentioned before, compared to other PDP phosphors, $BaMgAl_{10}O_{17}:Eu^{2+}$ is the most vulnerable material. Is quality decreases during panel processing and it degrades during operation. Degradation effects are mostly related to its host lattice and the Eu^{2+} activator ion. One of the main reasons for the severe decrease in light output is the oxidation of the Eu^{2+} ion. Oshio et al. confirmed in their work formation of $EuMgAln0_{19}$, in which the europium is trivalent. It is very inefficient in this lattice and thus hardly visible in the emission spectrum. Other degradation factors and mechanism will be presented in next chapter [7,18,19].

4. Degradation mechanisms of phosphors

In this chapter, mechanisms of luminance decrease in blue-emitting $BaMgAl_{10}O_{17}:Eu^{2+}$ phosphor will be examined. There are at least two stages in degradation of current phosphor fluorescence characteristics. First is observed during panel fabrication, second during panel life. Each process is quite complicated, and to understand them thoroughly means to understand how to improve radiation stability of phosphors.

4.1 Degradation due to thermal treatment effect.

It was shown experimentally, that those fluorescence characteristics degradation mechanisms of $BaMgAl_{10}O_{17}:Eu^{2+}$ phosphor during panel fabrication are due to annealing in the air, which leads to the oxidation of the dopant [20]. During the oxidation process, decrease of divalent europium concentration is followed by an increase in the trivalent europium concentration but also by a decrease in the pre-existing traps concentration. The degradation itself is due to three different mechanisms: the adsorption of an oxygen atom from the atmosphere into an oxygen vacancy of the surface phosphor, the diffusion of ions along the conduction layer of BAM and the transfer of one electron from dopant ions to adsorbed oxygen ions (when Eu^{2+} ions are close to adsorbed oxygen ions) [20,21].

$BaMgAl_{10}O_{17}:Eu^{2+}$ has a crystal structure similar to hexagonal β-alumina, $NaAl_{11}O_{19}$ (**Figs. 9, 11**).

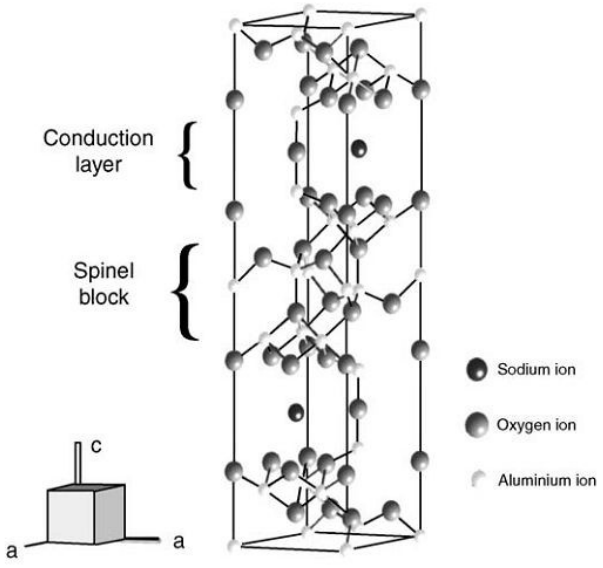

Figure 9. β-alumina crystalline structure: $NaAl_{11}O_{19}$ [20]

By one of the methods, BAM is synthesized via the substitution of Na^{+} ion in the conduction layer with the Ba^{2+}/Eu^{2+} ions and of the partial replacement of Al^{3+} ions by Mg^{2+} ions. For the Eu^{2+}-doped material, the Ba ions in the conduction layer is replaced by the Eu^{2+}. The phosphor shows then, with a high efficient luminescence, a broad band around 450 nm, corresponding to the $4f^{6}5d \rightarrow 4f^{7}$ transition [20].

The excitation spectrum of the BAM:Eu^{2+} (**Fig. 10**) reveals two different areas: one for the high energies (6.5-10 eV) corresponding to the lattice absorption and one for the lower energies (6-4.5 eV) due to the direct absorption in the dopant [23]. This last area shows two broad bands at around 240 and 310 nm due to the transitions between the ground state $4f^{7}$ and the crystal-field split $4f^{6}5d$ configuration [24].

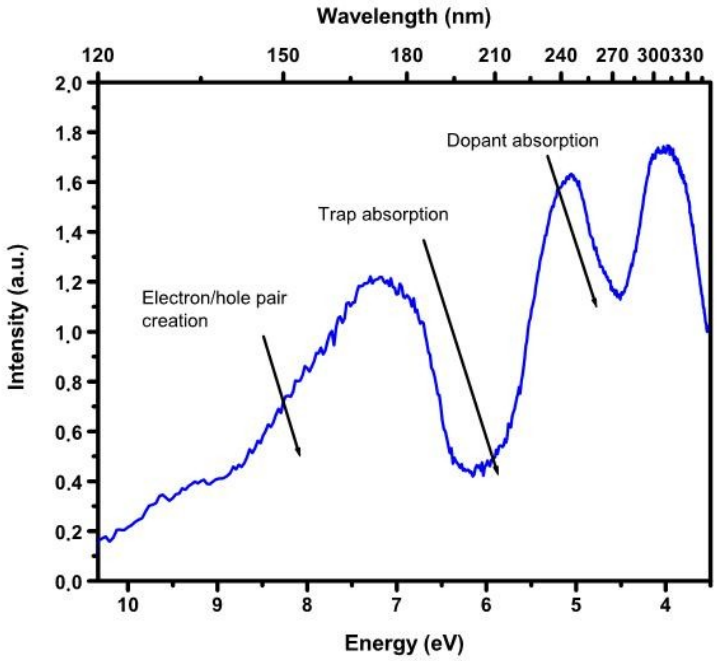

Figure 10. Excitation spectrum of $BaMgAl_{10}O_{17}:Eu^{2+}$. Excimer ArF laser (193 nm) used as an excitation source. [20]

Recently, electronic structure calculations of BAM:Eu^{2+} have been performed using the band structure approach and molecular orbital approach, respectively [25]. Their results indicated that Eu^{2+} ions occupy three different sites called Beevers-Ross (BR), anti-Beevers-Ross (aBR) and mid-oxygen (mO) sites. [24,26]

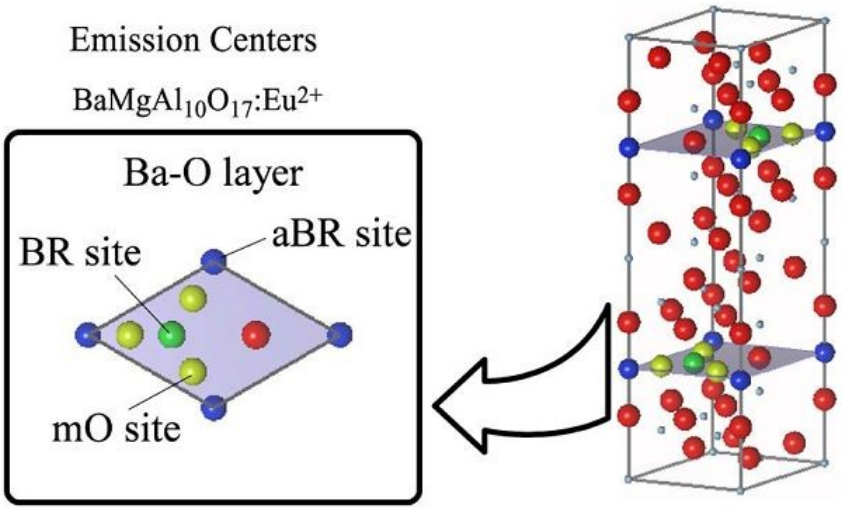

Figure 11. Crystal structure of BAM. [24]

The crystal structure of BAM shown in **Fig. 11** has the β-alumina structure. There are layers consisting of Ba^{2+} and O^{2-} ions between the spinel blocks and Eu^{2+} is generally believed to stay within these Ba-O layers. The positions of BR, aBR, and mO sites within this Ba-O layer are also shown in **Fig. 11.** The BR site is the substitutional site of Ba and the other two sites are interstitial sites.

The theoretical absorption spectra of Eu^{2+} at all three sites in BAM were obtained [24] and compared with the experimental excitation spectrum – three main peaks (a–c) and one sub-peak (b') are clearly identifiable. As shown in the **Fig. 12**, only the aBR site is contributing to peak **a**. These results indicate that in the actual material, the occupancy of aBR sites should be greater than the ones of the other sites [26].

Following assumptions, based on a structure similarity, help to understand the degradation mechanism:

• The β-alumina structure is a very good ion conductor. This crystalline structure induces the high mobility of the cation in the conduction layer. For BAM, this leads to the diffusion of the barium and europium ions along the conduction layer [20, 24].

• The electric charge compensation is only global inside the crystalline unit cell. Locally, the electric charge compensation is not respected. This characteristic is important and induces a creation of numerous traps during the synthesis of the phosphor. These traps are

mainly due to the delocalization of the cationic and anionic ions and therefore the formation of F and V centers. This point is particularly important for BAM – oxygen vacancies can be created in the conduction layer close to dopant ions (Ba/Eu-O layer) [20, 24].

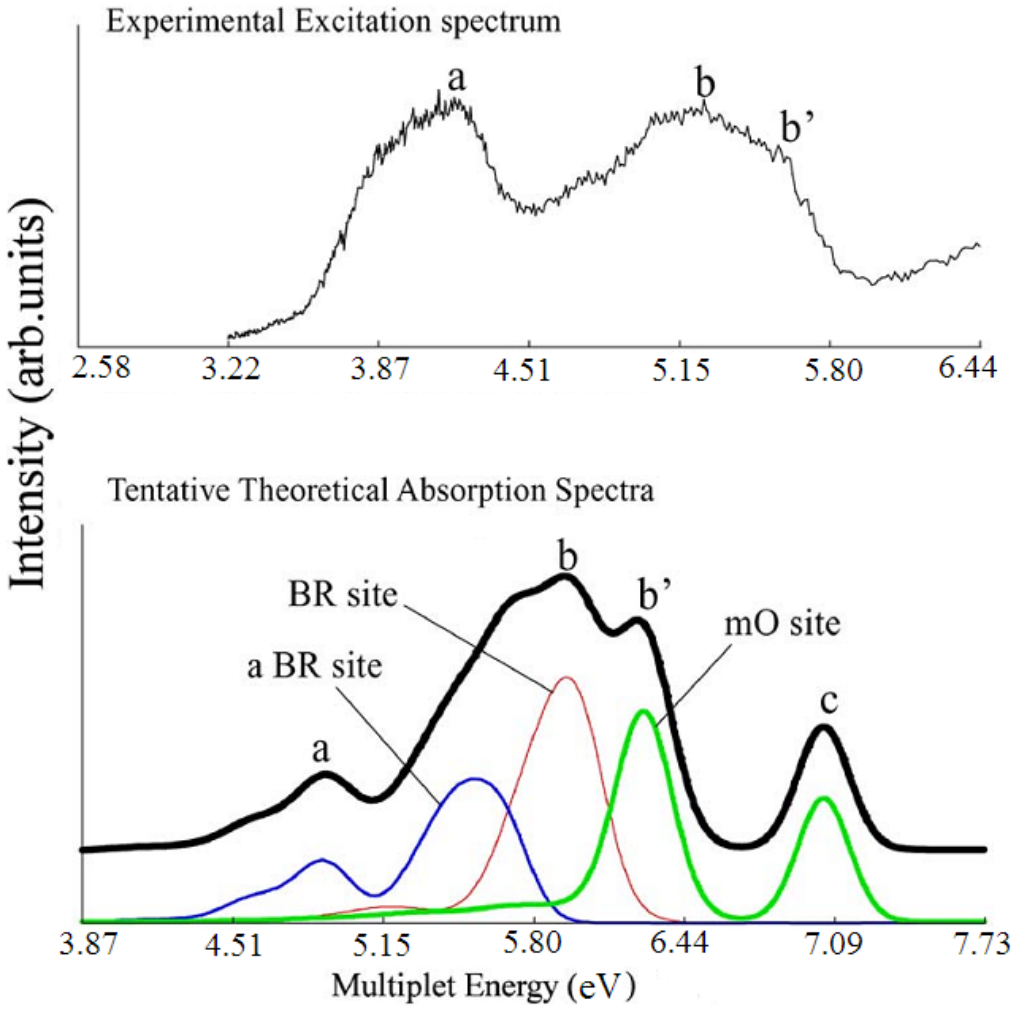

Figure 12. Experimental excitation spectrum and the theoretical absorption spectra for Eu^{2+} in BAM. The solid black line is a tentative spectrum produced by summing up the spectra for all three sites with relation of 1:1:1. [24]

Oxidation mechanism can be explained by considering three different processes:

• The adsorption of the gaseous oxygen atom in a oxygen vacancy of the phosphor lattice. In this case, the adsorbed oxygen is not in the same valency as the one of an oxygen ion of

the phosphor lattice. To be stabilized the adsorbed oxygen need to catch electrons. The adsorption mechanism obviously occurs at the phosphor surface.

• The diffusion through the conduction layer of the europium ions (due to the increase of the temperature during the thermal treatment).

• The electronic transfer from a divalent europium ion to adsorbed oxygen (when the two species are close to each other).

The adsorption process leads to the decrease of the oxygen vacancies and also the F/F^+ centers. The decrease in the Eu^{2+} ion luminescence intensity and the increase in the Eu^{3+} ion luminescence intensity are obviously due to the electronic transfer between an adsorbed oxygen (which catches two electrons to get into the O^{2-} valency) and the Eu^{2+} ions. The mobility of the Eu^{2+} ions is more important than mobility of oxygen vacancies. The process is likely to take place at the phosphor surface, because adsorbed oxygen ions are unable to diffuse quickly into the lattice [20,24,26].

The degradation mechanism is summarized in the following equation:

$$2Eu^{2+} + \frac{1}{2}O_2(g) + V_O \rightarrow 2Eu^{3+} + O_O^{2-},$$

where Eu^{2+} – a divalent europium ion, $O_2(g)$ – a gaseous oxygen atom, V_O – an oxygen vacancy, Eu^{3+} – a trivalent europium ion and O_O^{2-} – an oxygen ion of the lattice. [20]

4.1 Degradation due to VUV excitation.

Another type of mechanism of luminance decrease of phosphors is excitation by a Xe plasma discharge [1,27,28]. It has been shown experimentally, that the aging process is mainly due to the vacuum ultraviolet excitation (VUV). Depending on the temperature, this type of aging route can be separated in to two different processes: at low temperature, corresponding to the autoionisation of luminescent centers; and at high temperature, linked to the formation of traps in the phosphor [27]. These traps induce a perturbation of the energy migration in the phosphor. Noticeable parameters in the creation of traps are:

density of the VUV excitation, temperature, atmosphere and pressure surrounding the phosphor [28].

Many attempts were made to clarify and generalize the complex aging process during the operation of panels without explaining the real degradation of BAM. Most probable hypothesis is linked to the vacuum ultra violet excitation of the plasma discharge, but apparently from that, it have been proposed to explain the aging process with the bombardment of ions and interaction between the different compounds of a plasma cell and the phosphor [29,30].

In the works of B. Moine and G.Bizarri [1,27,28] it was shown, that during the aging process, no spectral changes are observed in emission spectra. As for excitation spectra (**Fig. 13**), the main difference (a decrease of the fluorescence intensity yield) between the reference sample and the irradiated one is situated in the high energy range (6.5-10 eV). As was mentioned before, this diapason corresponds to the lattice absorption.

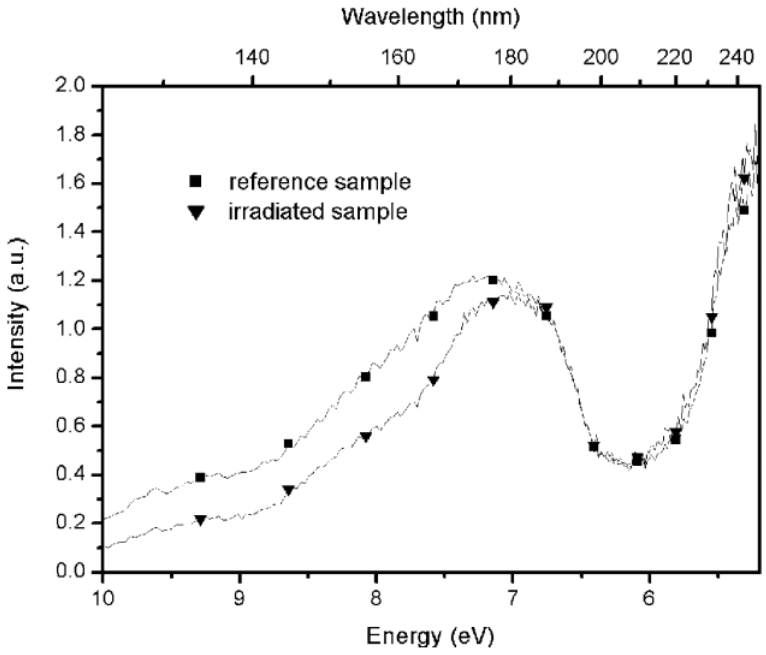

Figure 13. Excitation spectra recorded for two samples at room temperature: reference fresh BAM:Eu^{2+} sample and the sample irradiated by laser (193 nm, 100 μJ and 20 Hz during 2 h). [27]

Another method of analysis, which helps to understand degradation processes, is reflectance spectrum. The reflectance spectrum of a material is a plot of the radiation reflected as a function of the incident wavelength and serves as a unique signature for the material. Reflectance spectra were obtained for both previously mentioned samples (**Fig. 14**). Their structure is equivalent and corresponds to the one observed in the excitation spectra: two distinguishable areas, which are equivalent to the dopant and lattice absorption. A third absorption band is visible, from 200 nm to 220 nm, intensity of which increases after laser irradiation. Therefore, the aging process is likely to induce the creation of species, which absorb in this range of wavelength, but do not transfer the absorbed energy towards the emitting ions (since no increase of intensity is observed in the corresponding region of the excitation spectra) [27,31].

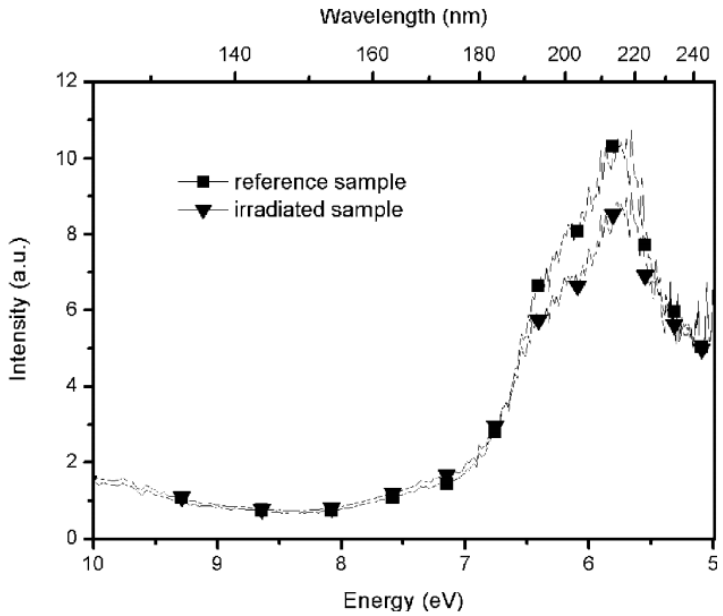

Figure 14. Reflectance spectrum recorded for two samples at room temperature: reference fresh BAM:Eu^{2+} sample and the sample irradiated by laser (193 nm, 100 μJ and 20 Hz during 2 h). [27]

From examples, it appears that the aging process does not correspond to a decrease of the concentration of divalent europium ions (as with thermal degradation) [32]. It corresponds either to a decrease of the efficiency of the energy transfer from the host matrices, or to the increase of the absorption of other centers which do not transfer their energy to the

divalent europium ions. So, the aging process is related to the vacuum ultraviolet excitation, which is mainly absorbed by the matrices and induces the creation of electron-hole pairs and to a modification of the energy migration inside the host matrices [33].

Experiments show, that the fluorescence intensity of BAM is sensitive to the excitation pathway. This means that the degradation occurs only via an excitation towards delocalized states (ionization or lattice absorption) [27]. Since the degradation seems to be linked to the migration of energy, it is likely that the role played by traps is of first importance [28]. If traps are involved in the process, temperature becomes a parameter that must influence the aging process. VUV excitation results in the formation of electron-hole pairs, which can be trapped either by the dopant ions or by the defects present [28]. When electron-hole pairs are trapped by a divalent europium ion a blue fluorescence should be observed; but trapping by a defect site will disturb energy transfer process, and will result in the loss of the energy of the electron-hole pair. If the aging process is only caused by to the filling of traps, it should be possible to empty the traps by increasing the temperature and consequently – to slow down the aging process. By a bleaching process at high temperature, initial intensity will be recovered [27].

At low temperature, even the shallow traps are able to capture the electron-hole pairs [27]. With increase of the temperature, traps must be situated deeper if they are to take part in absorption process. Therefore, by increasing temperature, the part of aging process due to shallow traps is reduced. This is a good explanation of degradation slowdown in temperature range of 120-500 K [27,34]. Combining the effects of VUV irradiation and of temperature, deep and stable traps are being created. They capture electron–hole pairs and lead to non-radiative recombination. The energy absorbed by the host matrices cannot reach the Eu^{2+} ions anymore. However, at higher temperature (700 K) the creation of traps is enhanced which in turn explains the acceleration of the degradation.

The VUV photons of the laser or of the Xe plasma discharge are primarily absorbed in the matrices of BAM, by moving an electron from the top of the valence band up to the conduction band [34]. The top of the valence band is essentially made of the orbital 2p of oxygen ions [24]. Furthermore, due to the very high absorption of VUV photons, the penetration depth of the exciting beam is very small (a few tens of nanometers). Therefore, it is reasonable to assume that the VUV excitation perturbs and ionizes the oxygen ions

which are close to the surface of the sample, leading to desorption of the oxygen atoms [20]. Thus, oxygen vacancies are created and they act as very efficient electron traps, inducing the formation of F/F^+ centers [27]. Consequently, VUV degradation mechanism is associated with an increase of the trap concentration and not with a decrease of the concentration of luminescent centers.

As for thermal quenching, it is concluded that the process is not due to a large displacement between the ground and excited states of Eu^{2+} (in the configuration coordinate diagram), also it is not explained by thermal release of a hole from Eu^{2+} to the valence band. The energy barrier for thermal quenching corresponds qualitatively with the energy difference between the lowest 5d state and the bottom of the conduction band. Most likely, it is due to thermal excitation of the 5d electron to conduction band states. The 5d electron remains bonded in a Eu^{3+} trapped exciton state from which it returns non-radiatively to the Eu^{2+} ground state [34,35].

Mechanisms of degradation, considered most important, have been discussed. Several possible mechanisms were shown for thermal degradation, as well as VUV degradation mechanisms (which also depend on the temperature – reversible at low temperature and irreversible at high). They are: localized fluorescence quenching from the 5d band levels of the divalent europium ions at high temperature; divalent europium ion auto-ionization process; involvement of traps in the fluorescence mechanism and decrease of the fluorescence efficiency due to the perturbation of the migration of the electron-hole pairs created by VUV excitation via non-radiative transition.

5. Synthesis process of a blue emitting $BaMgAl_{14}O_{23}:Eu^{2+}$ phosphor

5.1. Concept of what to be done

To understand degradation processes, increase luminous efficiency, lifetime, and color purity characteristics of phosphors, used in plasma display panels, many person-hours were already invested in various areas of research. At the Institute of Physics, University of Tartu, several suggestions were made and experiments were conducted.

It was offered to synthesize BAM crystals with an increased amount of matrix component Al_2O_3. Instead of $BaMgAl_{10}O_{17}:Eu^{2+}$ (BAM) all source compounds were taken in a proportion for $BaMgAl_{14}O_{23}:Eu^{2+}$. It was proposed, that by increasing amount of Al_2O_3 different quantities of emission centers, compared to typical BAM, could be formed. In addition, in compound with modified structure, intensity of degradation processes should decrease. Along with standard 10 mol percentage (mol %) of Eu^{2+}, structure with 5 mol % have been synthesized.

BAM septa-alumina phosphor has been a body of recent interest, but still a lot of information is missing. Phase diagrams needed for synthesis at the time of experiment, were not found and thermodynamics of synthesis process either. Presumably, component diagram for baking process of $BaMgAl_{14}O_{23}:Eu^{2+}$ should look like the one shown in the **Fig. 15**.

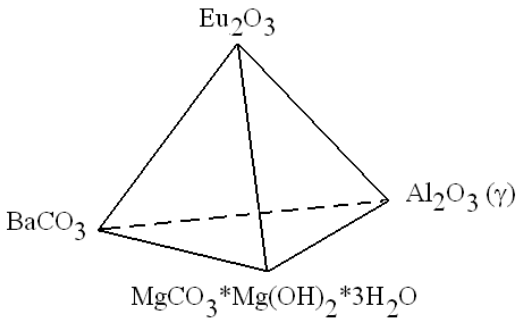

Figure 15. $BaMgAl_{14}O_{23}:Eu^{2+}$ component diagram.

5.2. Used laboratory apparatuses for synthesis

In order to synthesize needed compounds, common knowledge of laboratory operations was obligatory. Such as measuring and weighting of source compounds, mixing, and basic usage of laboratory glassware and of course maintenance of safety measures. Author of this thesis in person did not operate laboratory devices that can only be operated by a highly trained staff. One of such devices was GERO™ High Temperature Furnace. Let us briefly describe this state of art furnace.

Furnace installation structure consists of the following sub-assemblies: standard pipe furnace and control system. Furnace case represents electrically heated high-temperature furnace for a maximum continuous operation temperature of 1800°C. The furnace consists of an enamelled sheet steel case with covered power supply points in the interior of the case. Threaded plates are welded onto the bottom of the furnace, which are used for installation. Heating elements consist of a metal-ceramic material and an oxide component (predominately a vitreous phase). These elements are designed to stand a maximum process temperature of 1800°C. The heating cassette consists of a special steel sheet, which is encased by insulation and heating elements themselves. The furnace housing is cooled by means of convection.

Furnace modification, which was used in this experiment, includes additional Vacuum/Gas equipment. Compared to standard equipment, Vacuum/Gas extension allows us to work in vacuum or gas environment. It must be mentioned, that current furnace insulation is made of magnesium oxide elements and contains no asbestos wool. That makes it a part of environmentally friendly technology. A cross-section of furnace is represented in **Fig. 16** (scanned from furnace manual).

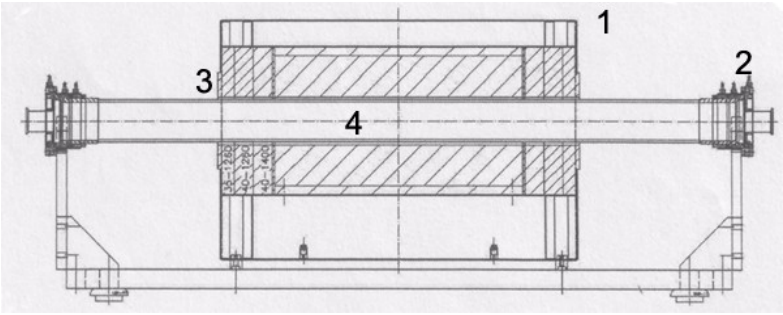

Figure 16. Cross-section of GERO™ High Temperature furnace. 1 – heat-resistant insulation layers; 2, 3 – hermetically tight joints; 4 – spalling-resistant metal ceramics tube.

5.3. Solid phase synthesis

Sintering is a method of making objects from powders by solid-state reaction, increasing the adhesion between particles as they are heated. It is one of the traditional methods for manufacturing phosphors for plasma display panels. Sintering and solid-state reactions are closely related to diffusion, which is very important in achieving uniform distribution and allocation of source compounds in final product [36].

First, amounts of source materials needed for our experiment were calculated. Two compounds were synthesized containing different amount of dopant. Those compounds were presented with numbers 67 and 68. Amount of source compounds for Mixture № 67 was calculated based on requirement, that it must have 5 mol % of Eu, and mixture № 68 therefore 10 mol % of Eu. Compounds that were synthesized should have the fallowing structures:

№ 67: $Ba_{0,95}MgAl_{14}O_{23}:Eu_{0,05}$ and № 68: $Ba_{0,9}MgAl_{14}O_{23}:Eu_{0,1}$

Source compounds that were used:

- Manufacturing Company: Alfa Aesar
- $BaCO_3$, Puratronic®, (High purity research chemicals and materials), purity of compound 99,997 %
- $MgCO_3 \cdot Mg(OH)_2 \cdot 3H_2O$, Puratronic®, purity 99.996 % (metals basis)
- Al_2O_3 (γ), purity of compound 99.997 %
- Eu_2O_3, REactor®, purity of compound 99.99 %

We need	0.95 BaO	MgO	$14 \cdot Al_2O_3$	Eu_2O_3	$Ba_{0,95}MgAl_{14}O_{23}$
We take	$BaCO_3$	$MgCO_3 \cdot Mg(OH)_2 \cdot 3H_2O$	$14 \cdot Al_2O_3$	Eu_2O_3	
	0.95·197.35	0.5 · 196.69g	14·101.96		
=	178.11g	98.35g	1427.44g		900.5
reduce ×150					
*	1.1874	0.6557g	9.5167g	0.0617g	6.0033g

Figure 17. Amounts of source compounds needed for synthesis of $Ba_{0,95}MgAl_{14}O_{23}:Eu_{0,05}$

We need	0.95 BaO	MgO	$14 \cdot Al_2O_3$	Eu_2O_3	$Ba_{0,9}MgAl_{14}O_{23}$
We take	$BaCO_3$	$MgCO_3 \cdot Mg(OH)_2 \cdot 3H_2O$	$14 \cdot Al_2O_3$	Eu_2O_3	
	0.95·197.35	0.5 · 196.69g	14·101.96		
=	178.11g	98.35g	1427.44g		893,64
reduce x150					
*	1.1874	0.6557g	9.5167g	0.1303	5.9576

Figure 18. Amounts of source compounds needed for synthesis of $Ba_{0,9}MgAl_{14}O_{23}:Eu_{0,1}$

Rows marked with a "*" symbol represent final amounts of source compounds, which were used it on our synthesis.

When the calculations were finished, needed amounts of source compounds were weighted on scales (with grade of accuracy ± 0.05 mg) and mixed together in a mortar. Mortar that was used during preparation of mixtures was made from alumina (Al_2O_3). Such mortar was chosen because of its higher durability compared to agathic (SiO_2) mortar. Mixing in agathic mortar should be avoided, because interchange between Si atoms (from mortar structure) and Al atoms (from Al_2O_3 structure) can occur. This will result in a decrease of purity.

After mixing dry powders, pure alcohol (96.7 %) was added into the mortar to increase interaction area between components, and to make mixture uniform. To achieve needed uniformity of mixture, mixing process itself took up 1.5 hours. To eliminate remains of alcohol and humidity, obtained mixture was put in thermostat for a period of 12 hours. Temperature of thermostat was 130ºC.

At this point, all preparations for sintering were done. Dried mixture was poured into sintering boat. Boat was made also from Al_2O_3, and previously was used only for synthesis of BAM compounds. During sintering, a part of Eu ions diffuse into the structure of boat, which reflects on amount of Eu^{2+} in a lower layer (marked in our experiments as C). Also, purity if sintering boat is between 99.5 - 99.7 % of Al_2O_3 – this can also be favorable for exchange processes. In upper layer (marked as A), concentration of Eu^{2+} ions partly lowered because of interaction with surrounding environment. Layer B,

which is sandwiched between layer A and C, will be the main object of investigation. Division into phases can be seen in **Fig. 19**.

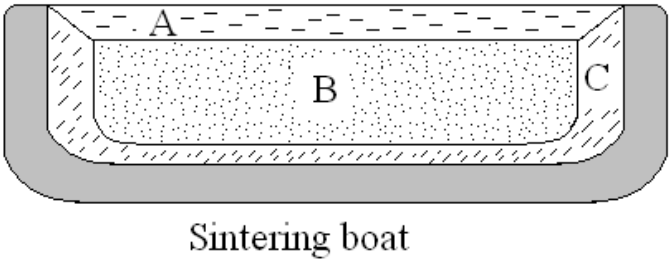

Figure 19. Division into phases in a sintering boat.

Next step, in sintering process, was to put boats with mixtures into high-temperature furnace GERO™. Boats were placed in furnace in following order, as shown in **Fig. 20**. This is so compound № 68, with higher concentration of dopant, will not affect compound with lesser concentration № 67.

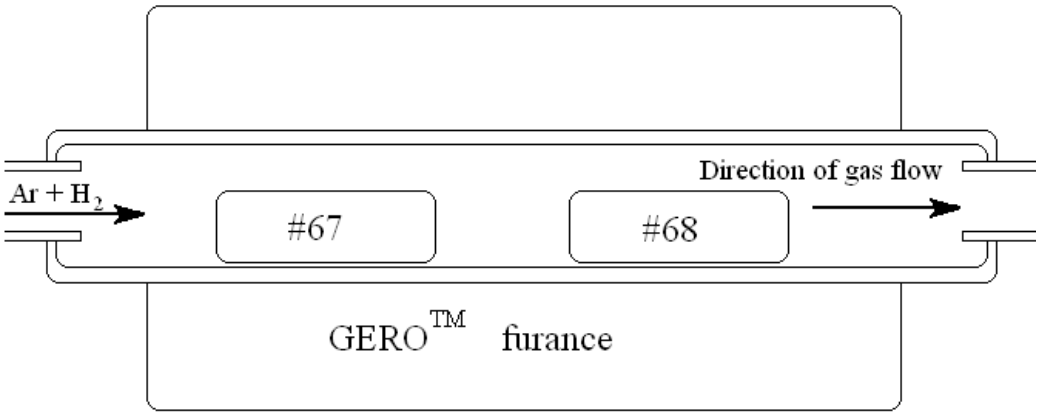

Figure 20. Positioning of boats in the furnace.

System was hermetically sealed, and heating chamber turned on. When temperature in furnace reached 150º C, pure Ar gas flow was introduced into system. This must be done, in order to blow through CO_2 and H_20 compounds, which occur as a source compound

disassimilation reaction products. Pure argon is blown through the system until temperature in heating chamber reaches 1550ºC (BAM, being synthesized at temperature 1400º C were not uniformly mixed, and traces of source compounds were found). At this point, 4 % of H_2 was added to Ar flow. H_2 gas is used as a reduction environment, which is needed to reduce dopant from Eu^{3+} state (Eu_2O_3) to needed Eu^{2+}. Fusion reaction itself lasted for 5 hours. This time was considered optimal. During that period, temperature was held constant at a point of 1550º C, and mixture of Ar and H_2 (96 % and 4 % respectively) was flowing through the system.

After 5-hour time, heating was turned off, and system is left to cool down independently. Cooling temperature-chart can be seen in **Fig. 21**. During cooldown chamber with boats was isolated in Ar/H_2 environment and gas flow was stopped. After temperature reached approximately 440º C, chamber was depressurized, because dopant oxidation was not possible anymore.

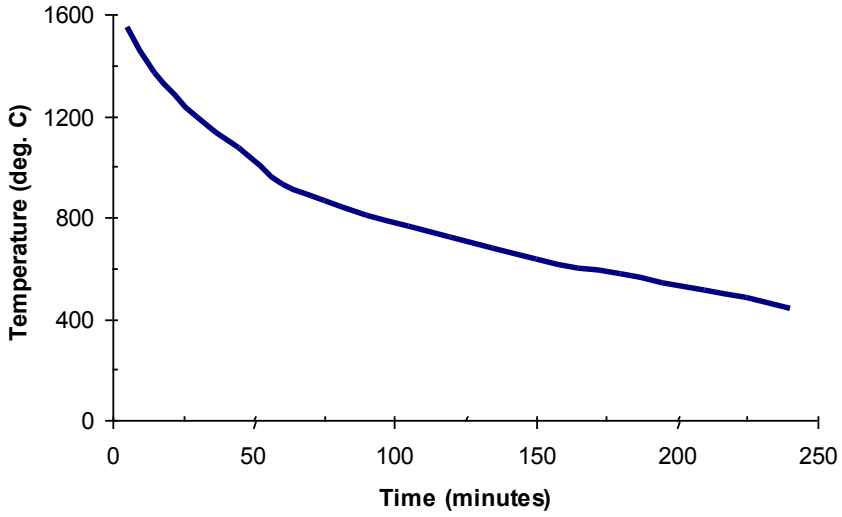

Figure 21. Cooling temperature-chart for GERO™ high-temperature furnace.

6. Setup of experiments

6.1 Methods of analysis

It is a very well known fact, that interaction of electromagnetic radiation with matter causes absorption, emission, and scattering of radiation. As a result of this interaction, we are able to characterize the optical properties of materials by measuring the properties of electromagnetic radiation. The spectroscopic techniques used in this work to measure different properties of electromagnetic radiation are discussed in this paragraph.

The most classic experiments in spectroscopy are concerned with the determination of the transition energies of the optical center [7]. So called transition "energies" are commonly expressed in terms of energy (eV), frequency ν (s^{-1}) or ω (rad s^{-1}), wavelength λ (nm), or wavenumbers $\tilde{\nu}$ (cm^{-1}). Physical magnitude measured is an intensity of electromagnetic radiation as a function of photon energy. A graph that plots the intensity versus photon energy is called a spectrum, and peaks (or dips) in the spectrum reveals the locations of optical transitions.

To perform an experiment, a (broadband) excitation source, light-dispersing elements, and a detector are needed. The sample is irradiated with radiation from the excitation source. When this radiation induces a transition to an excited state in the material (usually from the ground state) this may lead to emission of light from the sample. The detector is used to measure either the intensity of the emitted light or the intensity of the residual light from the excitation source.

Four techniques are commonly used for this kind of experiments: absorption spectroscopy, diffuse reflection spectroscopy, luminescent excitation spectroscopy, and emission spectroscopy. In absorption spectroscopy the photon energy of the radiation incident on the sample is selected by a scanning monochromator. Absorption spectroscopy is used to measure the transmitted signal for transparent (non-scattering) samples such as single crystals or solutions. An alternative for strongly scattering materials, such as polycrystalline powders, is diffuse reflection spectroscopy. The difference in set-ups for absorption and reflection spectroscopy is in the detection compartment. When diffuse reflection spectroscopy is used, the backscattered signal is detected and compared to the back-scattered signal from a reference material [7,37,38,39].

The two other techniques, emission and luminescent excitation spectroscopy, use the phenomenon that after excitation of the sample to an excited state the transition to the ground state results in the emission of light. Usually, emission and excitation spectroscopy are both performed in one set-up (**Fig. 22**) [7,37].

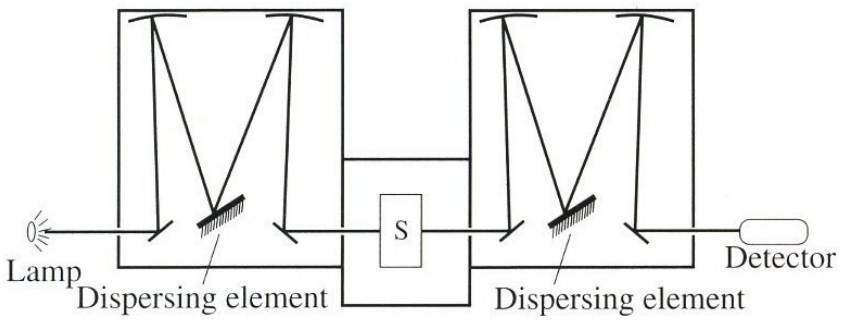

Figure 22. Schematic set-up for emission and excitation spectroscopy. [7]

It contains a broadband excitation source, a light-dispersing element for the excitation radiation, a sample compartment S, a light-dispersing element for the radiation emitted, and a sensitive detector for measuring the intensity of the radiation emitted. In emission spectroscopy, the emitted light is spectrally resolved by scanning the emission-dispersing element. The dispersing element for the excitation source remains fixed during scanning of the emitted light. An emission spectrum yields information on the energetic positions of the optical transitions that are involved in the emission of light. In excitation spectroscopy, the emission monochromator is set at a wavelength corresponding to a needed emission line and the excitation light is scanned. In contrast to an absorption spectrum, an excitation spectrum yields information on the energetic position of absorption bands that lead to emission of the chosen wavelength. Last technique can prove very valuable in studying specific absorption transitions (for example in the case when more than one optical absorbing species are present in the material) [7,38].

Excitation and emission spectroscopy have very low background levels and a much higher sensitivity. They are used in combination with samples containing very small quantities of luminescent species. Absorption and diffuse reflection spectroscopy have much larger background and noise levels and are used for more concentrated samples. Both types of techniques also show different requirements for the equipment used. For absorption and

diffuse reflection spectroscopy the requirements for the output powers of lamps and the sensitivity of the detector are less demanding than for emission and excitation spectroscopy. [7,38,39].

Another important method of research that was used is thermally stimulated luminescence (TSL) or thermoluminescence (TL). Thermoluminescence is the emission of light from an insulator or semiconductor when it is heated. This is not to be confused with the light spontaneously emitted from a substance when it is heated to incandescence. Thermoluminescence is the thermally stimulated emission of light following the previous absorption of energy from radiation. The three essential ingredients necessary for the production of thermoluminescence can be found in the following statement. Firstly, the material must be an insulator or semiconductor (metals do not exhibit luminescent properties). Secondly, the material must have at some time absorbed energy during exposure to radiation. Thirdly, the luminescence emission is triggered by heating the material. In addition, there is one important property of thermoluminescence. It is a particular characteristic of thermoluminescence that, once heated to excite the light emission, the material cannot be made to emit thermoluminescence again by simply cooling the specimen and reheating. In order to re-exhibit the luminescence the material has to be re-exposed to radiation, whereupon raising the temperature will once again produce light emission [40,41].

The fundamental principles that govern the production of thermoluminescence are essentially the same as those, which govern all luminescence processes, and in this way thermoluminescence is merely one of a large family of luminescence phenomena.

One of our main goals is to understand presence and creation of effects in BAM:Eu^{2+} crystals. In principle, experiments using thermoluminescence can be expected to yield useful information on the properties of various types of defect present within semiconductor (or an insulator). It is known that thermoluminescence is particularly sensitive to traces of impurities within the specimen. Already countless studies of the effect of impurities on thermoluminescence properties of various materials have been made.

In general, it is believed that the impurities give rise to the localized energy levels within the forbidden energy gap and that these are crucial to the TL process. When coupled with

the ability to separate the energies of these levels curves) thermoluminescence provides, in principle at least, a unique tool in the determination of the distribution of the defect energies. However, it is this very sensitivity of the method that makes interpretation of the results difficult. In addition to defect levels caused by extrinsic defects (i.e., impurities) there are also those due to intrinsic defects, such as lattice vacancies and interstitials. The presence of this type of imperfection is also crucial to the thermoluminescence process in many materials. Defects produced by the radiation itself may also be important. Also, studies have shown that in some samples the production of one thermoluminescent photon may involve several defect levels in a kind of cooperative effort. On the other hand, one type of impurity species may give rise to several thermoluminescence peaks. Investigations, which attempt to describe the defect state of a material by using thermoluminescence alone, are of limited value. The most progress in recent years has been made when several different methods have been used as an addition to thermoluminescence. Although it is fruitless to use thermoluminescence alone to describe the defect structure of a solid, it is a very useful technique when combined with other measurements. It is very rare that thermoluminescence provides no information at all [40,41].

6.2 Used laboratory equipment for experiments

The mechanism of luminance decrease of phosphors excited by a Xe plasma discharge has been described in second chapter. It has already been shown experimentally that the aging process is connected to the vacuum ultraviolet excitation. Series of experiments to accelerate degradation by using X-rays have been made. Based on excitation, emission, thermoluminescence and ageing by X-ray excitation, the main causes of the $BaMgAl_{14}O_{23}:Eu^{2+}$ degradation are going to be demonstrated.

To irradiate the objects, standardized X-ray source URS-1.0 was used. Radiation treatment was carried out at room temperature. X-ray tube is based on tungsten anticathode, and accompanying apparatus allows varying current strength (I) from 2 to 20 mA and voltage (U) from 25 to 55 kV. In our experiments we used I = 10 mA and U = 50 kV.

As for excitation of objects with radiation similar to the one being used in PDP (Xe resonance emission line, 147 nm) - we used vacuum monochromator VMR-2 with water

cooled D_2 (heavy hydrogen) discharge lamp (which allows to get intense radiation in the area of 4 -14 eV). From this range, we can separate similar radiation to Xe discharge (with photon energy of 8.43 eV). Part of our objects was irradiated only under this excitation energy.

To measure high-temperature thermoluminescence, SYSTEM 310 TLD Reader was used. The System 310 is a dosimetry (TLD) measurement instrument, which processes thermoluminescent materials and dosimeters to report exposure to radiation. Sample measurement temperatures of up to 500º C are achieved by direct high current heating and measuring the infrared (IR) emissions from the removable heating element. Real time data acquisition is realized by using a dedicated microprocessor – monitor and control the measurement sequence. N_2 gas was used to reduce the measurement background. Obtained TL data is presented as an optical glow curve and a temperature plot presented in graphical form versus time. To make measurements comparable, each component was placed in to a separate mount. Inner diameter of mount was 3 mm, and included compound layer thickness was 0.35-0.4 mm. Samples prepared by the same method were used in most of experiments.

Short-wavelength spectra of cathodoluminescence (CL) in powders were measured using a double prism vacuum monochromator DMR-4, a photomultiplier Hamamatsu R6838 and an electron gun (6 keV, 30 nA / 1 μA). Various pulse durations were used.

The excitation spectra of photoluminescence were measured in the region 5-11 eV using a vacuum monochromator VMR-2 and conventional photoelectric methods [42]. The emission and excitation spectra were corrected for the monochromators transmittance and the sensitivity of the photomultiplier [43].

To compile a proper knowledge base not only synthesized compounds ($Ba_{0,95}MgAl_{14}O_{23}:Eu_{0,05}$ and $Ba_{0,9}MgAl_{14}O_{23}:Eu_{0,1}$) were analyzed with described techniques. A whole series of related compounds, which were previously synthesized at the Institute of Physics, Tartu University, and also purchased source compounds were analyzed. More than a hundred of various measurements, ranging from 20 seconds to 340 minutes were made. Analyzed compounds are listed in the following table:

№/Name	Corresponding formula	№/Name	Corresponding formula
67(a,b,c)	$Ba_{0,95}MgAl_{14}O_{23}:Eu_{0,05}$	20	$BaMgAl_{14}O_{23}$
68(a,b,c)	$Ba_{0,9}MgAl_{14}O_{23}:Eu_{0,1}$	32	Al_2O_3
10	$Ba_{0.999}MgAl_{10}O17:Eu_{0.001}$	65(b)	$BaMg_{0.93}Al_{10}O_{17}:Mn_{0.07}$
12	$BaMgAl_{10}O_{17}$	59(b)	$Ba_{0.997}MgAl_{10}O_{17}:Eu_{0.003}$
19	$Ba_{0.99}MgAl_{14}O_{23}:Eu_{0.01}$		

7. Results and discussion

7.1 Thermoluminescent analysis of synthesized compounds

First compounds that are going to be discussed are № 67 ($Ba_{0,95}MgAl_{14}O_{23}:Eu_{0,05}$) and № 68 ($Ba_{0,9}MgAl_{14}O_{23}:Eu_{0,1}$). Samples were prepared form layer B (**Fig. 19**). Contaminated parts of synthesized compounds (A, C. **Fig. 19**) are not going to be observed in current work. Powders were pressed into round (ø 1, 3 or 5 mm) flat supports made from copper. If various compounds are represented on the same figure – this means that parameters of the experiment are the same, and powder samples are of the same size (unless stated otherwise).

As was mentioned before, X-rays were used to excite materials, and also to speed up degradation processes. When compound absorbs a high-energy quantum of X-ray radiation, this process results in the formation of wide set of low-energy electronic excitations. Some of this excitations model the effect of Xe discharge radiation. But, unlike VUV photons, X-ray quanta penetrate much deeper and that possibly will result in some noticeable differences in obtained results when compared to VUV. Exposure range to the X-radiation varied from several seconds to several hours. By changing exposure time to radiation it shall be possible to suggest dose-response correlation in the samples.

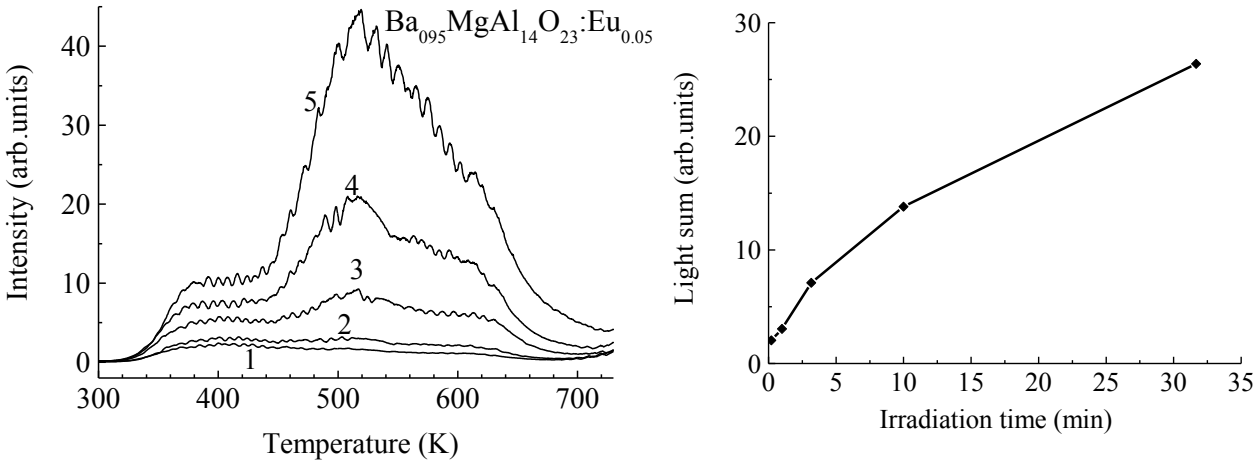

Figure 23. TL glow-curves and the curve of TL light sum dependence on irradiation time for sample № 67 (b) ($Ba_{0,95}MgAl_{14}O_{23}:Eu_{0,05}$). The duration of X-irradiation (295 K, 50 kV, 10 mA): curve 1 - 20 s, curve 2 - 60 s, curve 3 - 196 s, curve 4 - 600 s, curve 5 - 1900 s. Heating rate is $\beta = 2.86$ K s^{-1}.

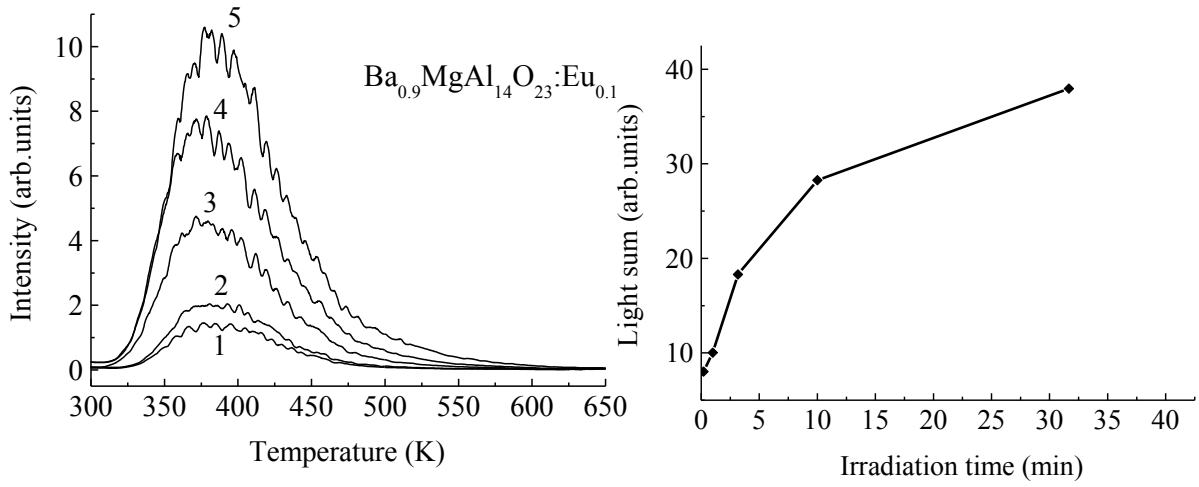

Figure 24. TL glow-curves and the curve of TL light sum dependence on irradiation time for sample № 68 (b) ($Ba_{0,9}MgAl_{14}O_{23}:Eu_{0,1}$). The duration of X-irradiation (295 K, 50 kV, 10 mA): curve 1 - 20 s, curve 2 - 60 s, curve 3 - 196 s, curve 4 - 600 s, curve 5 - 1900 s. Heating rate is $\beta = 2.86$ K s^{-1}

The temperature, at which the peak maximum appears, is related to the trap depth. In **Figs 23** and **24**, three different groups of peaks with the maxima at ~ 380 K, ~ 515 K and ~ 620 K. observed. This indicates that three different species of traps are being activated within this particular temperature range, each with its own trap depth value. In general, the larger the value of trap depth, the higher the temperature at which the peaks will occur (however, this might be not the case, and we will return to discussion of that aspect later). The area under each peak is related to the number of filled traps, which, in turn is related to the amount of radiation initially absorbed by the specimen.

Comparison of TL glow-curves and light sums shows, that compound with 5 mol % of Eu have all three peaks with sufficiently high amount of energy stored. This compound transforms incident energy into emission worse than a compound with twice as many quantity of Europium. It is possible to suggest, that its radiation stability is four times smaller than that of a compound with 10 mol %, because amount of energy stored is four times greater. We will try to prove this later, with experiments on vacuum monochromators.

With this description of the thermoluminescence process it is possible to observe all the essential elements of thermoluminescence made in the previous paragraphs, namely, the energy band model associated with the material; the absorption of energy from radiation

building up a population of trapped electrons; and the thermally stimulated release of the electrons followed by recombination and luminescent emission.

7.1.2 Analysis of the compounds directly related to septa-alumina BAM

In order to understand trapping processes better and to determine what peaks are connected with europium we will analyze several related compounds. Let us start with compounds № 19 ($Ba_{0.99}MgAl_{14}O_{23}:Eu_{0.01}$) doped with 1 mol% of Eu, and № 20 ($BaMgAl_{14}O_{23}$), which was not doped with Eu and represents pure septa-alumina BAM.

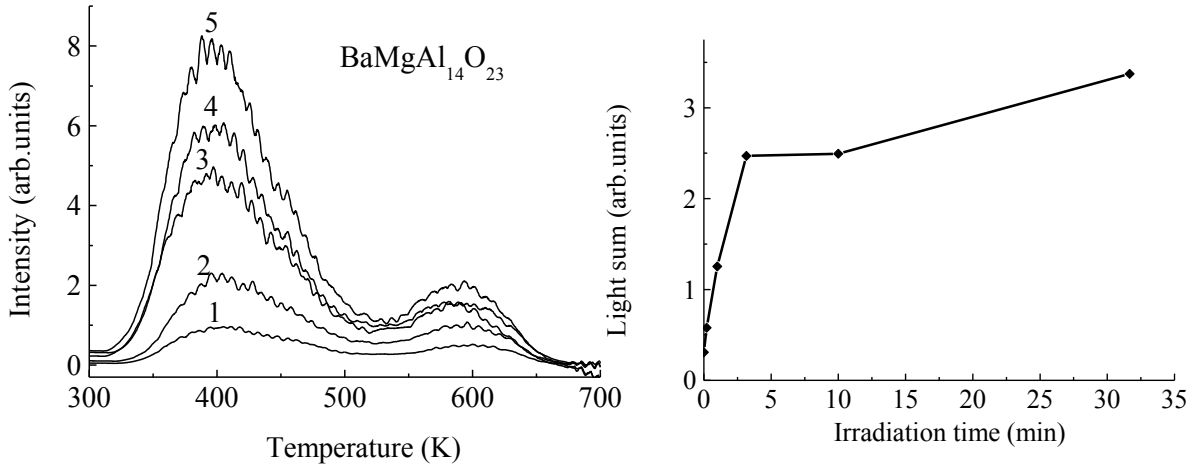

Figure 25. TL glow-curves and the curve of TL light sum dependence on irradiation time for sample № 20 ($BaMgAl_{14}O_{23}$). The duration of X-irradiation (295 K, 50 kV, 10 mA): curve 1 - 20 s, curve 2 - 60 s, curve 3 - 196 s, curve 4 - 600 s, curve 5 - 1900 s. Heating rate is $\beta = 2.86$ K s^{-1}.

Peak at ~ 400 K is similar to that shown on **Fig. 24**, but is situated at slightly higher temperature. This little shift to lower temperature in $Ba_{0,9}MgAl_{14}O_{23}:Eu_{0,1}$ can be explained by presence of significant amount of europium. Traps emit absorbed energy at lower temperature and thus need less energy for the process. This also means that they are situated closer to the surface of energy gap. In addition, if we compare intensities of those

two peaks, we will notice that they are not that different. Peak from the same temperature region in $Ba_{0,95}MgAl_{14}O_{23}:Eu_{0,05}$ (**Fig. 23**) also has similar intensity difference compared to $BaMgAl_{14}O_{23}$. Therefore, it is possible to assume, that some Eu ions take part in formation of that peak.

As for peak situated at ~ 600 K in $BaMgAl_{14}O_{23}$, it is absent in $Ba_{0,9}MgAl_{14}O_{23}:Eu_{0,1}$ but is very brightly represented in $Ba_{0,95}MgAl_{14}O_{23}:Eu_{0,05}$. It is possible that thermoluminescence concentration quenching is responsible for that process, and shallower traps tend to absorb most of the irradiated energy, so defects that are situated deeper do not take part in the process. Also, with increased concentration, there are other types of defects which tend to accumulate all of the energy, and it is possible that deep situated defects transform incident radiation, and don't take part in degradation processes.

At first, experiments with standard setup were performed on $Ba_{0.99}MgAl_{14}O_{23}:Eu_{0.01}$, but due to unexpectedly high TL intensity we had to downsize sample support by two times, and decrease current strength from 10 mA to 5 mA.

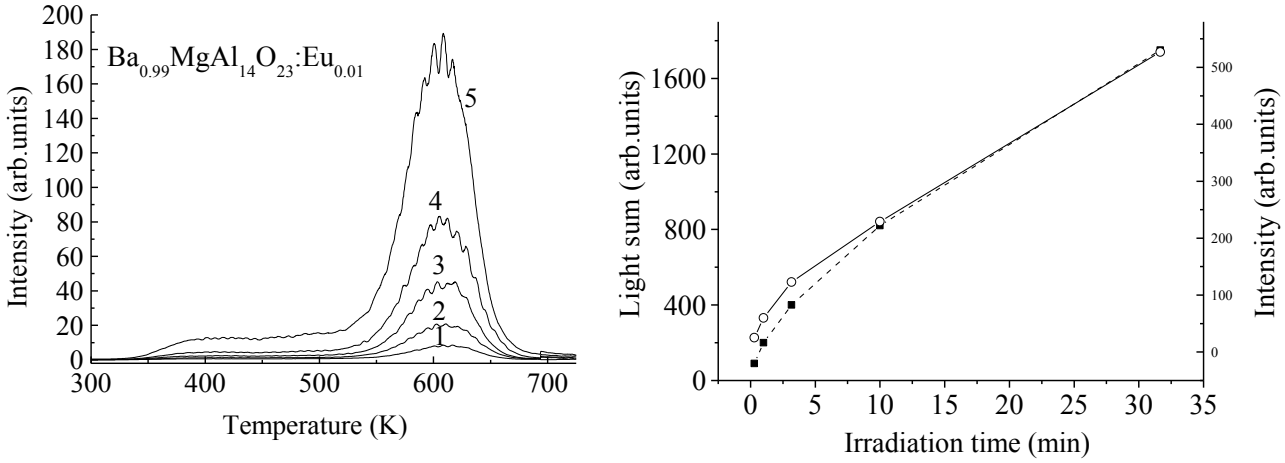

Figure 26. Sample № 19 ($Ba_{0,99}MgAl_{14}O_{23}:Eu_{0,01}$). TL glow-curves and the curves of TL light sum (●) and 600 K TL peak intensity (○) dependence on X-irradiation time (295 K, 50 kV, 5 mA). Duration of irradiation: curve 1 - 20 s, curve 2 - 60 s, curve 3 - 196 s, curve 4 - 600 s, curve 5 - 1900 s. Heating rate $\beta = 2.86$ K s^{-1}

From **Fig. 26** we can see a drastic increase in intensity of ~ 600 K peak. This peak is observed in the compound that is note subjected to impurity and in the compound with 5 mol % of dopant, while it is absent in the compound with 10 mol % of europium. Doping with 1 mol % is certainly responsible for such remarkable increase in peak intensity. So, it is possible to assume, that Eu^{2+} ions are uniformly distributed in the compound, and are situated in the most stable and favorable position.

Data from the last experiment is suitable to show another interesting correlation. **Fig. 27** represents the process of accumulation of light sum, in conditions where probability of recombination process during irradiation time is high. Light sum accumulation in such conditions should follow square root dependence from irradiation time [44,45].

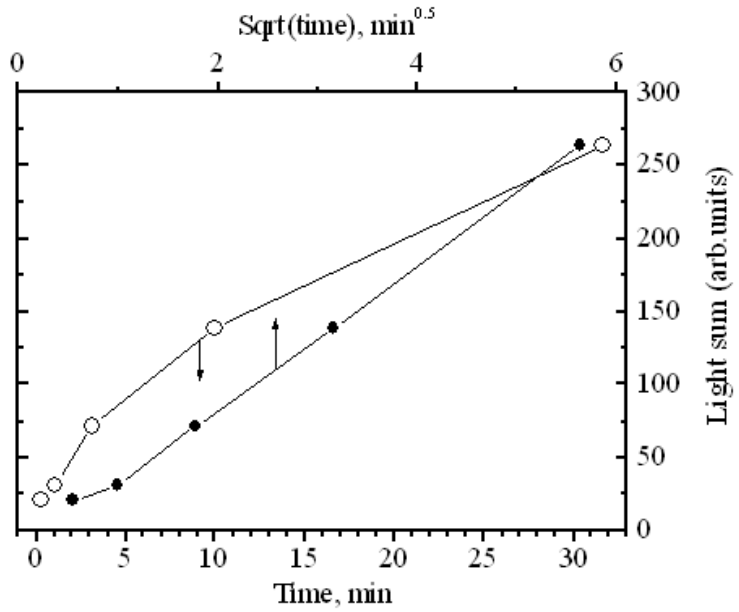

Figure 27. Dependences of TL light sum accumulation from irradiation time for sample № 19 ($Ba_{0,99}MgAl_{14}O_{23}:Eu_{0,01}$). ● – square root dependence; ○ – conventional dependence on irradiation time.

This dependence is not so well observed in current case, and a possible reason for that is saturation of traps. Also, it is probable, that recombination processes do take place, and there is a high probability of degradation processes. Furthermore, intensity (in approximation) is directly correlated to the trap concentration but also to the recombination center concentration. So when we notice a decrease in the thermoluminescence intensity, this evolution cannot be attributed simply to the signature

of a decrease in the trap concentration, and oxidation mechanism of Eu^{2+} should also be linked to the process [20].

7.1.3 Trap characteristics obtained by fading experiments

A quick way for obtaining qualitative information about the trap characteristics of a thermoluminescent material consists in the comparison between glow-curves recorded at different time intervals after irradiation [40]. The following **Fig. 28** shows the glow-curves of sample 67(b), irradiated with X-rays for 1900 seconds. Glow-curve 1 has been recorded immediately after X-irradiation (2 minutes after irradiation had been stopped); the second is the glow-curve recorded 216 hours after the end of the irradiation (so called dark pause; object was stored in opaque container and at room temperature). The third plot is the difference between the two previous glow-curves: this difference gives the indication of the TL lost during fading as a function of the glow-curve temperature.

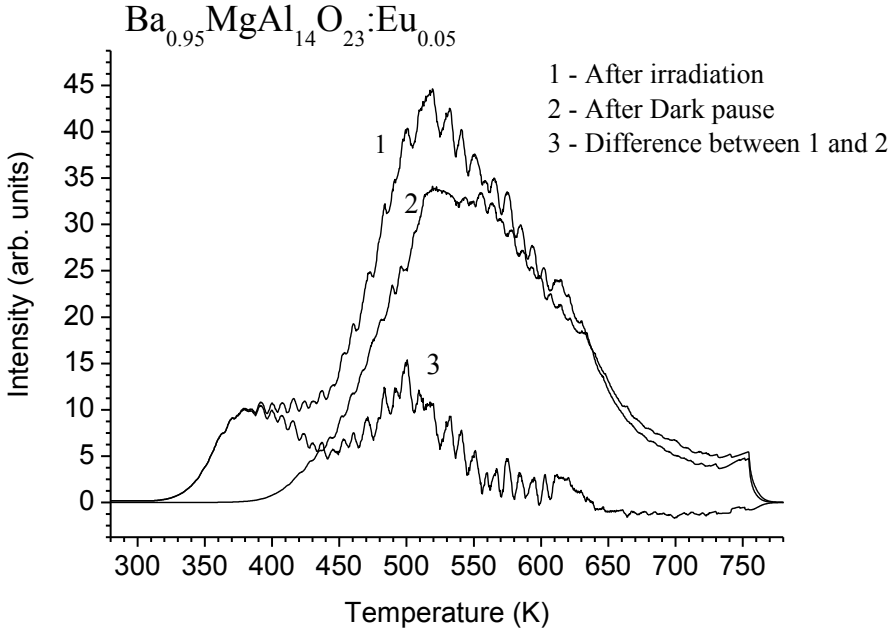

Figure 28. TL glow-curves for sample № 67(b) ($Ba_{0,95}MgAl_{14}O_{23}:Eu_{0,05}$) after X-irradiation (295 K, 50 kV, 10 mA, 1900 s). Curve 1 – immediately after irradiation, curve 2 – after dark pause, curve 3 – difference between two previous glow curves. Heating rate is $\beta = 2.86\ K\ s^{-1}$.

Supposing the fading is an isothermal decay at room temperature, and is given by following equation:

$$I = I_0 \exp(-\lambda t),$$

where I_0 is the TL emission recorded immediately after irradiation, I is the TL after the fading time t, and λ is the decay constant of the process. From this follows an equation:

$$\lambda = -\frac{1}{t} \ln\left(\frac{I}{I_0}\right).$$

Fig. 29 represents the plot of the resulting values of λ as a function of the glow-curve temperatures. In this figure, it is possible to identify three different regions. In the first region decay constant λ decreases as the glow-curve temperature increases; in the second region a clear area of stability is observed and, finally, a third region, above 700 K, where the results are highly scattered because I and I_0 are more or less quite similar. The behaviour of λ in the first region is a clear indication of a continuous distribution of trapping levels, whereas the flat region indicates a single trapping level [40,41].

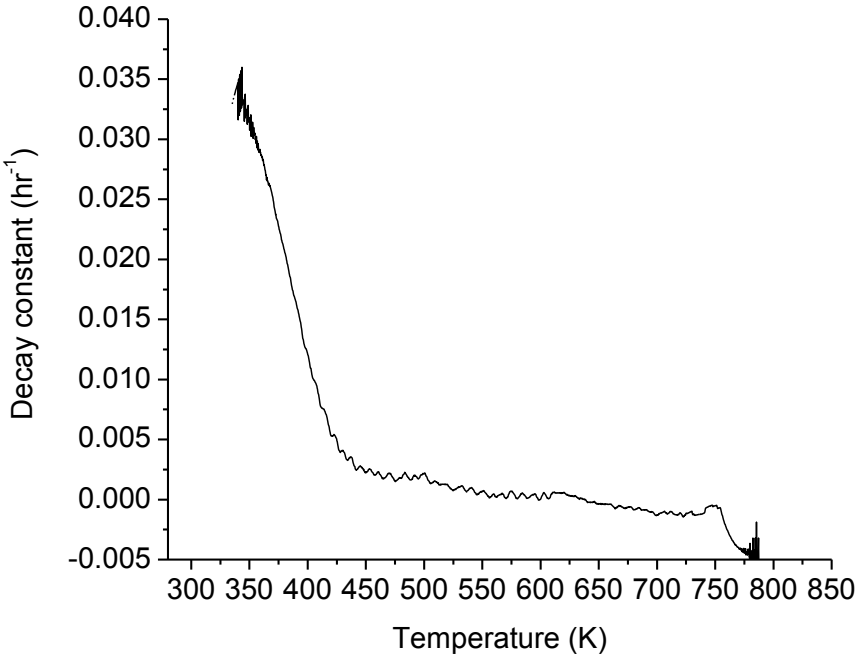

Figure 29. Decay constant as a function of the temperature.

Within the time of selected dark pause, peak that used to show at ~ 390 K totally disappears. Peak, which was measured at 500 K, changes its light sum approximately by 15 percent. 600 K peak almost had not changed. For a low-temperature peak, possible reason for fading could be tunnel processes and closeness to storage temperature of 300 K. for a peak of 500 K, the reason for peak weakening could only be recombination tunnel processes [41].

The defects responsible for glow-peaks at 390 K and 500 K are somewhat close to each other. This can occur when traps and recombination centers are in a high concentration and when the two centers belong to the same defect site. This transition occurs through the potential barrier (tunneling) which separates electron from hole. The recombination results in the emission of luminescence, and thus fading. The effects are athermal.

7.1.4 BAM and related compounds

It is important to analyze other related compounds in order to see if the similarities between them exist. In this paragraph, we will stop on following compounds: № 12 – $BaMgAl_{10}O_{17}$, № 10 – $Ba_{0.999}MgAl_{10}O17:Eu_{0.001}$ and № 32 – Al_2O_3.

Fig. 30 shows TL curves obtained for ordinary, so called penta-alumina BAM. Comparing TSL curves obtained for septa-alumina BAM (**Fig. 25**), it can be seen, that the nature of peaks is similar, even though ~ 600 K peak is not that well presented. The difference in intensity of the peaks can be attributed to the difference in structure – with configuration of septa-alumina BAM being more compact – possibility of defects increase, as well as possibility of recombination processes during irradiation.

By doping this BAM with 0.1 mol % Eu^{2+} we will obtain another compound (№ 10) that is similar to № 19. **Fig. 31** resembles **Figs. 25** and **30**: we can see processes that are characteristic to both undoped BAM (~ 390 K peak) and those that are Eu doped samples (~ 600 K peak). Energy stored by a compound is noticeably smaller. Still, vast amount of recombination processes occur in the area of 600 K peak. It is noticeable, that the introduction of europium ions into the structure causes the increase of total TL light sum and as well as the appearance of additional TSL peaks.

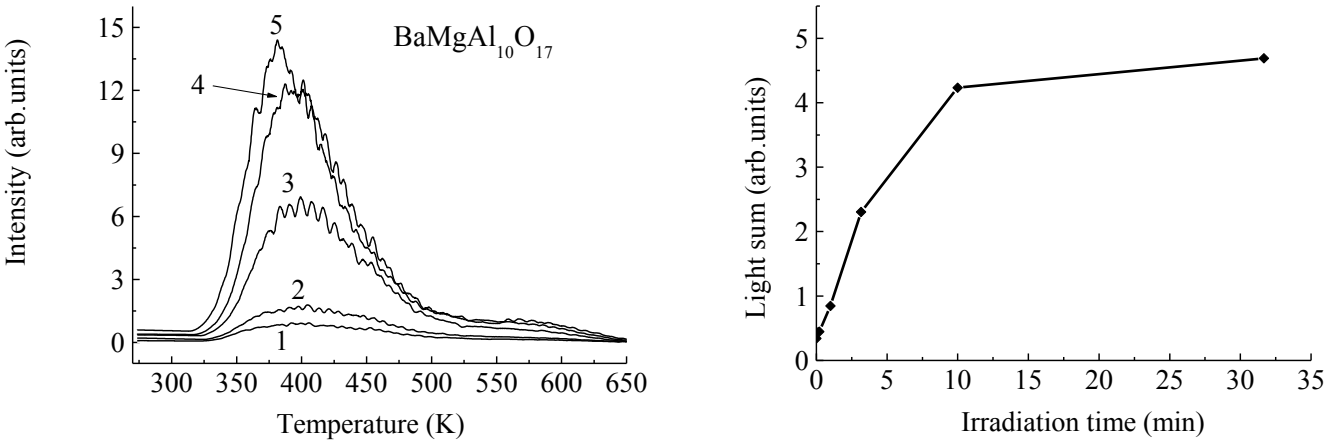

Figure 30. TL glow-curves and the curve of TL light sum dependence on irradiation time for sample № 12 ($BaMgAl_{10}O_{17}$). The duration of X-irradiation (295 K, 50 kV, 10 mA): curve 1 - 20 s, curve 2 - 60 s, curve 3 - 196 s, curve 4 - 600 s, curve 5 - 1900 s. Heating rate is $\beta = 2.86$ K s^{-1}.

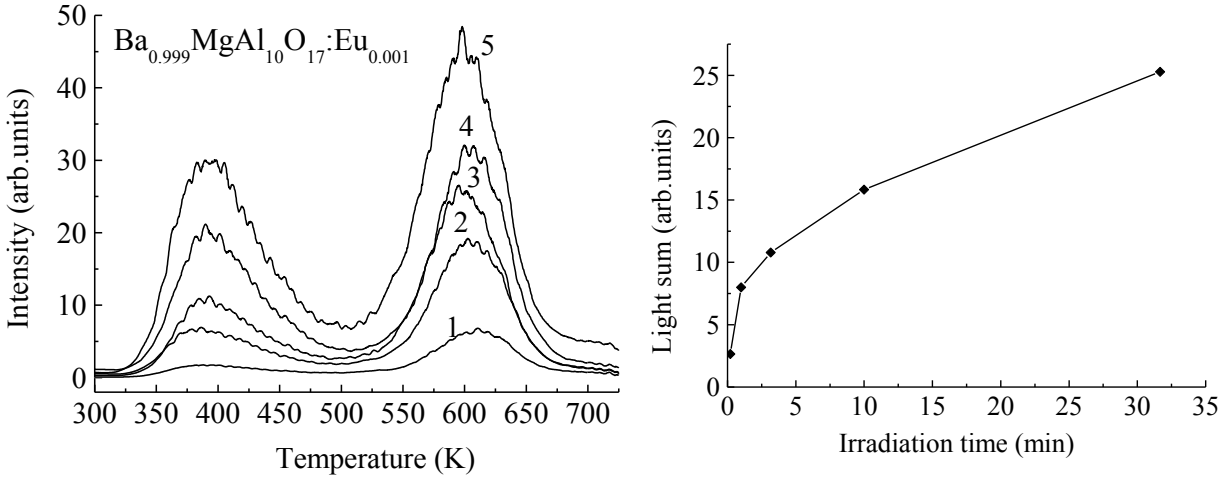

Figure 31. TL glow-curves and the curve of TL light sum dependence on irradiation time for sample № 10 ($Ba_{0,999}MgAl_{10}O_{17}:Eu_{0,001}$). The duration of X-irradiation (295 K, 50 kV, 10 mA): curve 1 - 20 s, curve 2 - 60 s, curve 3 - 196 s, curve 4 - 600 s, curve 5 - 1900 s. Heating rate is $\beta = 2.86$ K s^{-1}.

It is reasonable to have a look at how behaves one of the main crystal yielding components – Al_2O_3 (**Fig. 32**). All three of the TL peaks are represented. In addition, shift

by ~ 50 K of typical peaks occurs. Noticeable different is that the saturation of traps occurs much faster when compared to other compounds. 350 K and 570 K area maxima do not show such tendency.

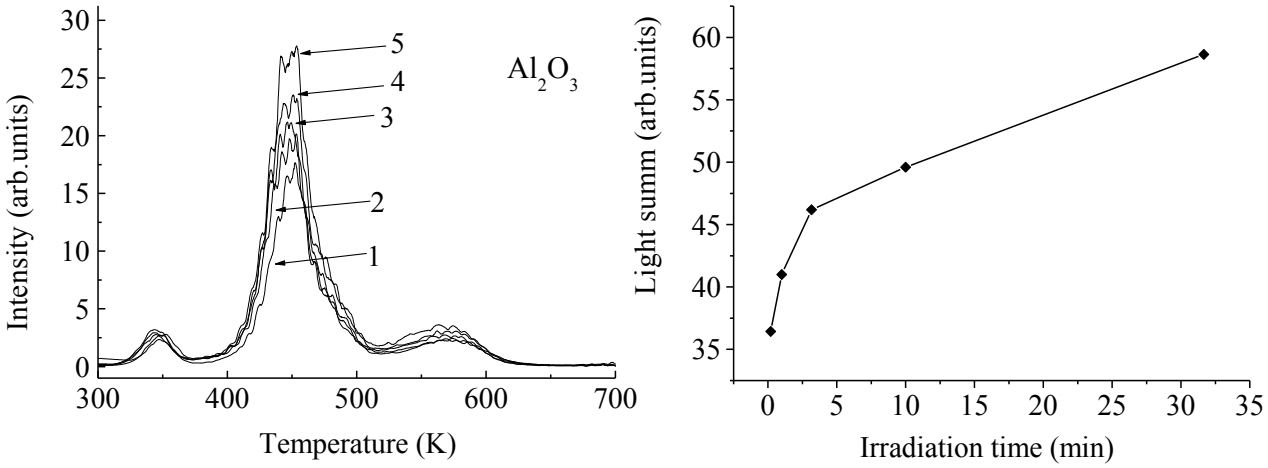

Figure 32. TL glow-curves and the curve of TL light sum dependence on irradiation time for sample for Al_2O_3 (№ 32). The duration of X-irradiation (295 K, 50 kV, 10 mA): curve 1 - 20 s, curve 2 - 60 s, curve 3 - 196 s, curve 4 - 600 s, curve 5 - 1900 s. Heating rate is $\beta = 2.86\ K\ s^{-1}$.

7.1.5 Degradation due to X-irradiation

Next goal was to show what parts of TL spectra are extra sensitive to X-ray radiation. We have decided to irradiate compounds of interest with three hour dose. All selected powders were packed into supports with ø 1 mm. We had to decrease the size of support, so that the amount of stored energy would still be measurable by our TLD Reader. Before irradiating our samples, every single one was annealed, so that all previously stored light-sum would be erased. We then selected a standard (test) dose of X-irradiation – room temperature (295 K), 55 kV, 10 mA for 196 seconds. After irradiation, samples were left to "cool down" for two minutes and TL spectra were obtained. The next step was to damage our test objects. For such purpose, we used X-rays with following parameters – room temperature (295 K), 55 kV, 20 mA for 10800 seconds (3 hours). Difference between test and damage dose of radiation is approximately 100 times. After damaging dose, samples are once again left to "cool down" for two minutes. Before annealing, we decrease

sensitivity of TLD Reader and then obtain TL spectra (not represented on charts). Last step in this experiment was to irradiate objects with test dose once again and obtain TL. Heating rate for all of our TL spectra is $\beta = 2.86$ K s^{-1}.

It has been shown by G. Bizarri and B. Moine, that the evolution of the thermoluminescence spectra is equivalent either for the surface traps, 193 nm laser excitation, as for the volume traps, X-ray irradiation [20]. This means, that our experiment sort of models damage done by prolonged VUV excitation. Following set of diagrams represents obtained results.

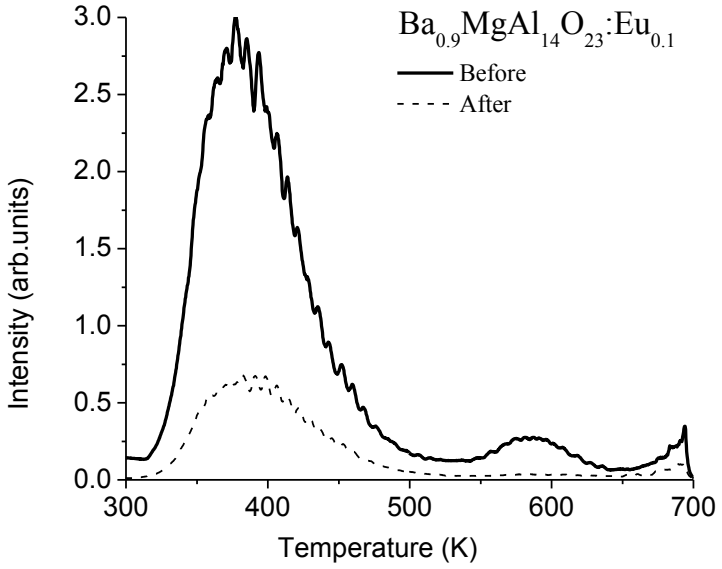

Figure 33. TL glow-curves for sample № 68(b) ($Ba_{0,9}MgAl_{14}O_{23}:Eu_{0,1}$) after test dose of X-irradiation (295 K, 55 kV, 10 mA, 196 s.). The measurements are made before (solid line) and after (dashed line) damaging dose (see text for details).

From **Figs. 33 – 38**, we can see that all glow-curves are suppressed, and there is almost no selective effect observed – all of the peaks are damaged proportionally. We can see that the thermoluminescent glow-curves are still caused by the recombination of three kinds of defects. The results of repeated irradiation prove that X-rays create no additional lattice defects, but already present defects are being damaged. As additional lattice defects are usually more stable, the defect concentration in big dose irradiated and then annealed sample would be higher than that in the unexposed sample. If they were actually created, they would have presented themselves in a thermoluminescence output.

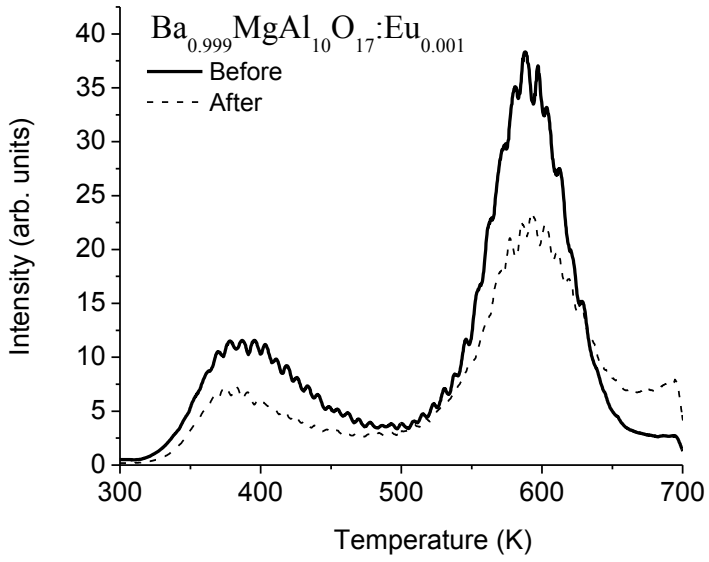

Figure 34. TL glow-curves for sample № 10 ($Ba_{0,999}MgAl_{10}O_{17}:Eu_{0,001}$) after test dose of X-irradiation (295 K, 55 kV, 10 mA, 196 s.). The measurements are made before (solid line) and after (dashed line) damaging dose (see text for details).

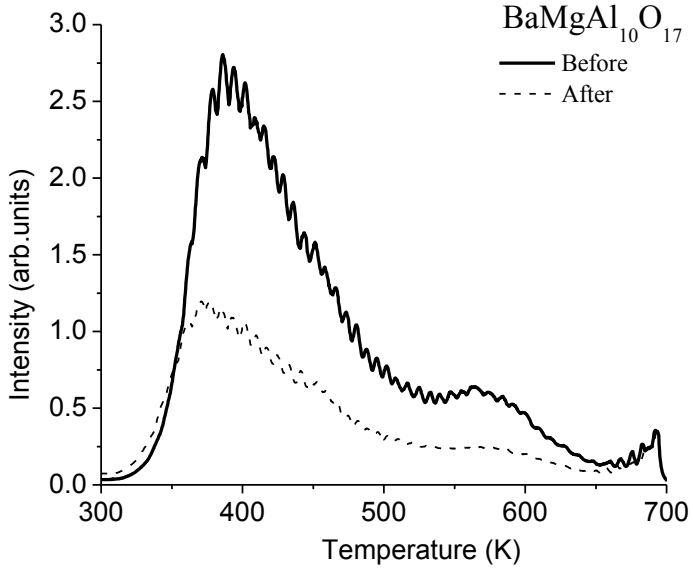

Figure 35. TL glow-curves for sample № 12 ($BaMgAl_{10}O_{17}$) after test dose of X-irradiation (295 K, 55 kV, 10 mA, 196 s.). The measurements are made before (solid line) and after (dashed line) damaging dose (see text for details).

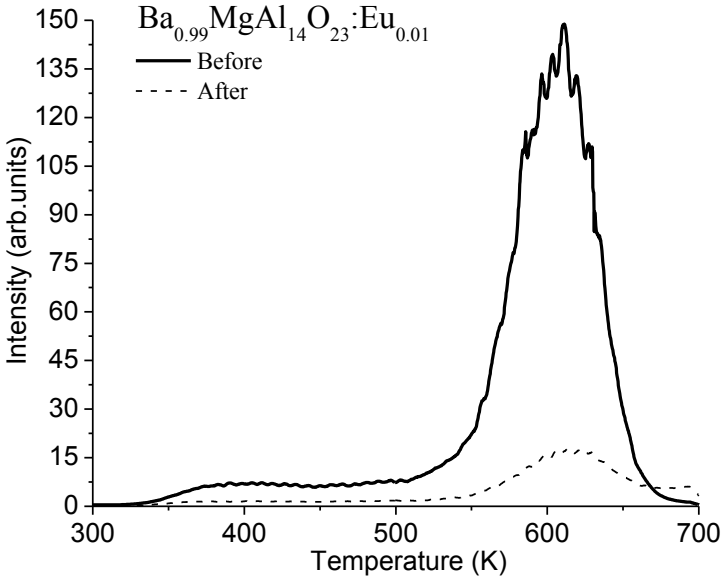

Figure 36. TL glow-curves for sample № 19 ($Ba_{0,99}MgAl_{14}O_{23}:Eu_{0,01}$) after test dose of X-irradiation (295 K, 55 kV, 10 mA, 196 s.). The measurements are made before (solid line) and after (dashed line) damaging dose (see text for details). TL intensity near the top of solid curve was registered with two different sensitivity settings and then re-calculated to the settings used in other experiments.

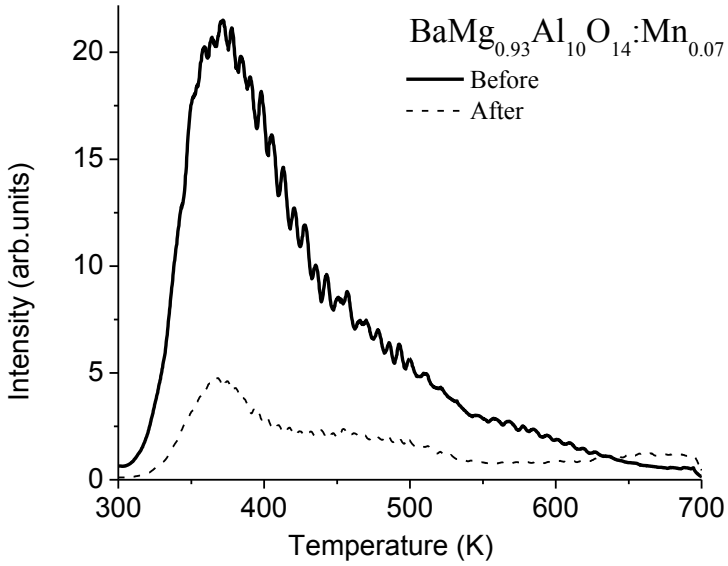

Figure 37. TL glow-curves for $Ba_{0,93}MgAl_{10}O_{14}:Mn_{0,07}$ (sample № 65(b)) after test dose of X-irradiation (295 K, 55 kV, 10 mA, 196 s.). The measurements are made before (solid line) and after (dashed line) damaging dose (see text for details).

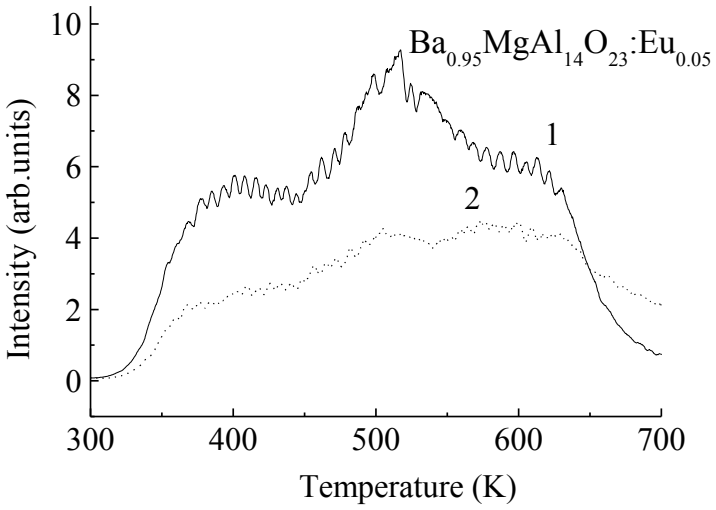

Figure 38. TL glow-curves for sample № 67(b) ($Ba_{0,95}MgAl_{14}O_{23}:Eu_{0,05}$) after test dose of X-irradiation (295 K, 55 kV, 10 mA, 196 s.). The measurements are made before (solid line) and after (dashed line) damaging dose (see text for details).

Comparison of **Fig. 34** and **Fig. 36**, shows, that $Ba_{0.999}MgAl_{10}O17:Eu_{0.001}$ is more stable to radiation than $Ba_{0.99}MgAl_{14}O_{23}:Eu_{0.01}$. This can be explained by difference in dopant concentration – if there are less impurity ions there are less traps, and they are less likely to be damaged. Another interesting aspect is that the light-sum of $Ba_{0,9}MgAl_{14}O_{23}:Eu_{0,1}$ decreased by 75 %, light-sum of $Ba_{0.99}MgAl_{14}O_{23}:Eu_{0.01}$ decreased by 76 %, for $Ba_{0,95}MgAl_{14}O_{23}:Eu_{0,05}$ it is 53 %, but for $Ba_{0.999}MgAl_{10}O17:Eu_{0.001}$ it is only 25%. Unfortunately, we have not measured commercially available penta-alumina BAM (5 mol % and 10 mol % Eu^{2+} content) in that experiment.

In order to know more about the radiation-induced defects and recombination centers that are responsible for TL, additional information on spectral distribution of TL emission is necessary. Generally, such information can be obtained during direct measurements of emission spectra in various TL peaks. In following paragraph, we will try to look on this problem from another angle.

7.2 Emission and excitation spectra

Before going on to analysis of data, obtained on various monochromator setups, it is interesting to have a look at TL spectra that were measured after irradiation of four samples (№ 67, № 68, № 10 and № 19) by VUV photons through a vacuum monochromator. Energy of photons used was 8.43 eV (147 nm), i.e. the same as resonant Xe discharge emission. Approximate amount of fallen photons on each sample was 1.2×10^{14}.

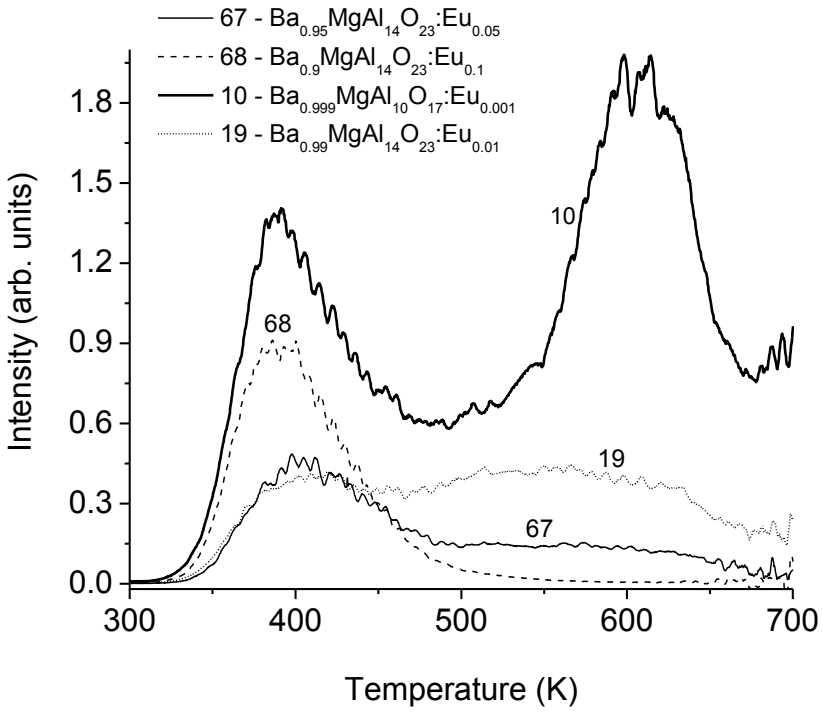

Figure 39. TL glow-curves measured for samples № 67 ($Ba_{0,95}MgAl_{14}O_{23}:Eu_{0,05}$), № 68 ($Ba_{0,9}MgAl_{14}O_{23}:Eu_{0,1}$), № 10 ($Ba_{0.999}MgAl_{10}O_{17}:Eu_{0.001}$), № 19 ($Ba_{0.99}MgAl_{14}O_{23}:Eu_{0.01}$) previously irradiated by 8.43 eV photons at 295 K during 30 minutes. Heating rate is $\beta = 2.86$ K s^{-1}).

Peaks are similar to those presented in previous paragraphs – therefore, the same traps are involved under both X-ray and VUV irradiation. In compound № 67 ($Ba_{0,95}MgAl_{14}O_{23}:Eu_{0,05}$), the ~ 500 K TL peak is hardly detectable, while it was dominant on previous TSL curves (see, e.g., **Fig.** 28). Thus, the energy accumulation under X- or VUV irradiation occurs differently. Compound №19 ($Ba_{0.99}MgAl_{14}O_{23}:Eu_{0.01}$) manifests

similar behaviour in respect of ~ 600 K peak. In compounds № 68 ($Ba_{0,9}MgAl_{14}O_{23}:Eu_{0,1}$) and № 10 ($Ba_{0.999}MgAl_{10}O_{17}:Eu_{0.001}$), the shape of glow-curves after VUV-irradiation coincide with those after X-ray excitation (see, **Figs.** 26, 31).

Being the object of interest, $Ba_{0,9}MgAl_{14}O_{23}:Eu_{0,1}$ (№ 68) was subjected to more experiments. Interesting glow-curve was obtained after irradiating one of the samples with 9 eV photons for 50 minutes (see **Fig. 40**).

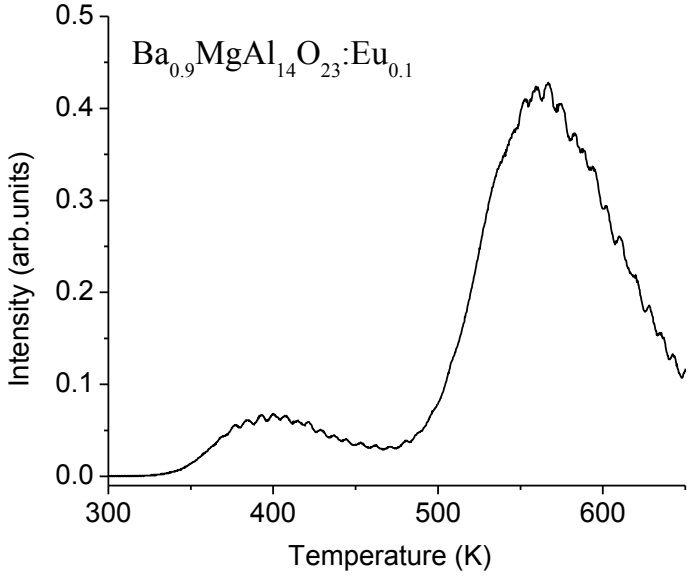

Figure 40. TL glow-curve for sample № 68 ($Ba_{0,9}MgAl_{14}O_{23}:Eu_{0,1}$) after irradiation by 9 eV photons for 50 minutes at 295 K. heating rate is $\beta = 2.86$ K s^{-1}

A completely new ~ 560 K peak is observed. Even after irradiating the same compound with X-rays, nothing similar has been noticed. For some reasons, different set of traps is active. It was reported already, that in the VUV irradiated BAM, the radiant efficiency shows a very sharp decrease when the excitation wavelength is shorter than 175 nm (excitation is 138 nm/ 9 eV in our experiment). The efficiency of impurity luminescence depends on the excitation mechanisms involved below and above the bandgap of BAM host lattice.

Another example of damage done by a high dose of radiation is presented on **Fig. 41,** which shows the excitation spectra for Eu^{2+} emission (selected by an optical filter C3C-22) in the sample № 68 ($Ba_{0,9}\cdot MgAl_{14}O_{23}\cdot Eu_{0,1}$) preheated to 700 K (curve with

filled triangles) and additionally irradiated by X-rays (empty triangles) for 1.5 hour. In the irradiated sample, the luminescence efficiency decreases in the region of 6.5-7.8 eV. According to the literature, the 170-nm band corresponds to the excitation of the host lattice. It can be suggested, that the bandgap of $Ba_{0,9}MgAl_{14}O_{23}:Eu_{0,1}$ host lattice (tentatively, for Ba-O layers) is situated near 165 nm (7.5 eV). When the excitation energy is higher than the bandgap of $Ba_{0,9}MgAl_{14}O_{23}:Eu_{0,1}$ host lattice (wavelength shorter than 165 nm), the exciting photons are absorbed by the phosphor host, and then the energy is transferred to Eu^{2+} ions. However, Eu^{2+} ions can be directly excited when the excitation photon energy is less than the bandgap of BAM host [46,47]. For the comparison, the luminescence excitation spectrum for a phosphor doped with a different impurity ion (Mn) is presented in **Fig. 41** as well.

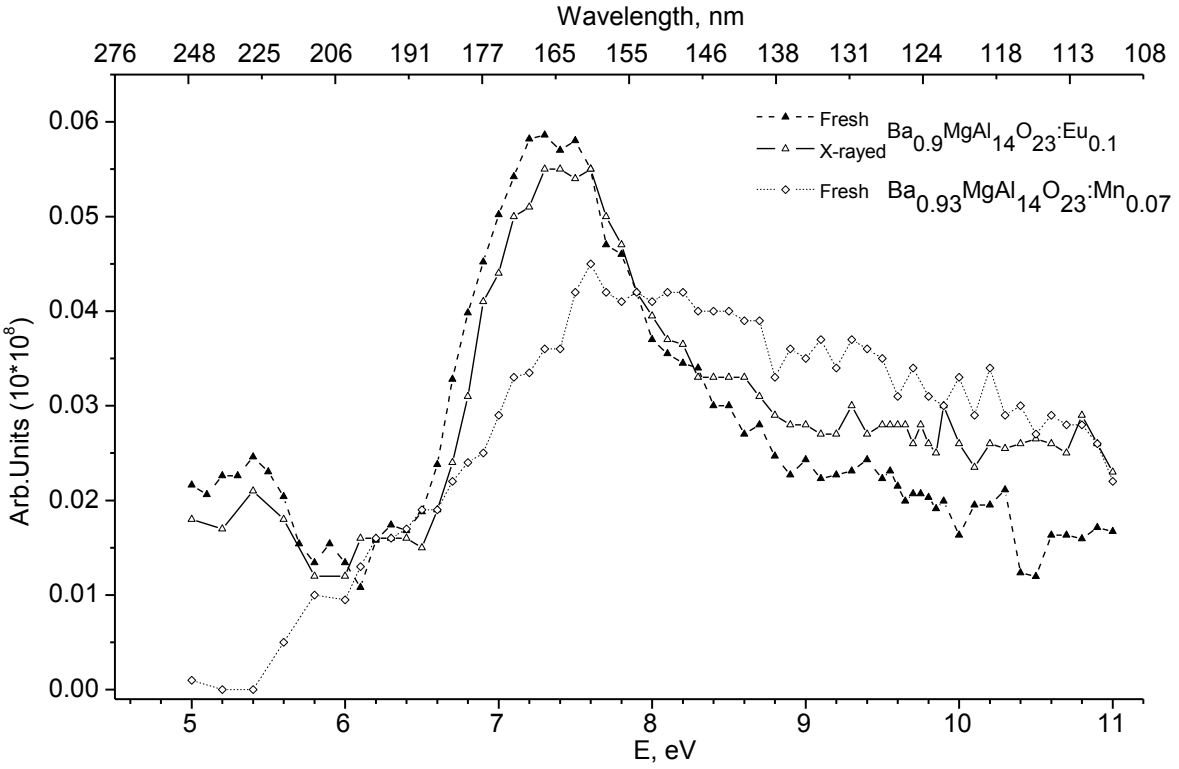

Figure 41. Excitation spectra for blue europium (Eu^{2+}) emission, measured for the sample № 68(b) ($Ba_{0,9}\cdot MgAl_{14}O_{23}\cdot Eu_{0,1}$) after preheating to 700 K in TLDR device (▲) and after additional X-irradiation (△) (55 kV, 20 mA, for 1.5 hours). The excitation spectrum for fresh and preheated $BaMg_{0.93}Al_{10}O_{17}:Mn_{0.07}$, (sample № 65, curve ◇, optical filter C3C-21). All experiments were conducted at T = 300 K.

In **Fig. 41**, peak situated at 5.5 eV is responsible for the transitions between the ground state $4f^7$ and the crystal-field splitted $4f^6 5d$ configuration of Eu^{2+} ions. If we compare fresh sample and irradiated samples, we will see, that increase of emission intensity is observed for X-irradiated object in the region of 8.4 eV to 11 eV. Interesting observation is that emission intensity is equal at 8.4 eV point for both fresh and irradiated samples. This is the region of resonant xenon discharge emission, and our test object is not affected by irradiation in this part of energy spectrum [20,31,47].

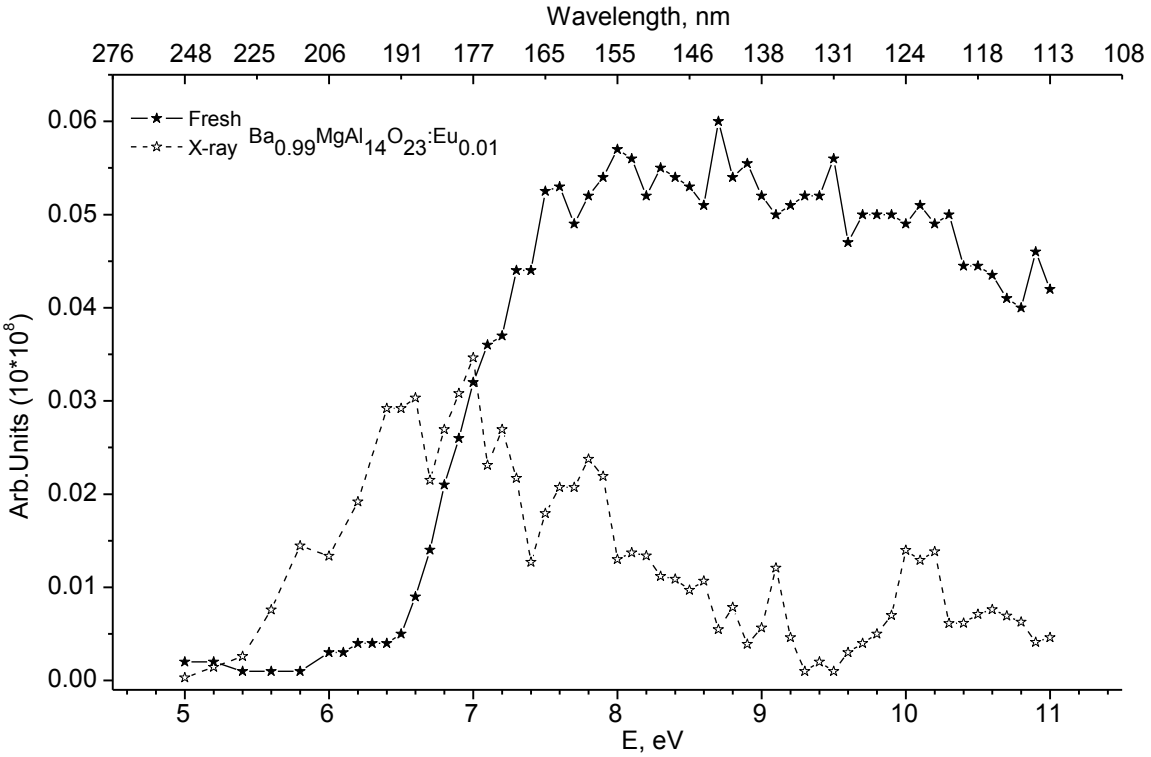

Figure 42. Excitation spectra for blue europium (Eu^{2+}) emission, measured for the sample № 19 ($Ba_{0.99}MgAl_{14}O_{23}:Eu_{0.01}$) after preheating to 700 K in TLDR device (★) and after additional X-irradiation (☆) (55 kV, 20 mA, for 1.5 hours). Experiments were conducted at T = 300 K.

The influence of X-irradiation on the impurity luminescence efficiency was additionally tested on a BAM compound with different amount of Eu^{2+} ions (see **Fig. 42)**. In the sample with smaller amount of impurities, the differences in the excitation spectra before and after irradiation are even more pronounced. From **Fig. 41** and **Fig. 42** we can state,

that a $Ba_{0,9}{\cdot}MgAl_{14}O_{23}{\cdot}Eu_{0,1}$ compound (10 mol % of Eu^{2+}) is more stable than $Ba_{0.99}MgAl_{14}O_{23}:Eu_{0.01}$ (only 1 mol % of dopant).

From **Fig. 41** and **Fig. 42** it can be seen that the aging process is associated with important decrease in the energy transfer efficiency from the host matrices to the emitting centers. It is proposed, that the main reason is essentially the defect density and the formation of traps in the host material. When an energy quantum is absorbed, it creates an electron–hole pair. Then the electron may be trapped by a defect and the energy absorbed is not transferred to the emitting centre. This also leads to the formation of color centers (samples changed color from white to brown). The aging process is not simply associated with the filling of traps but with the creation of additional traps and energy migration among these traps, leading to a non-radiative recombination. In our case, these traps are created in a whole body of the sample because of the penetration depth of the X-rays [48].

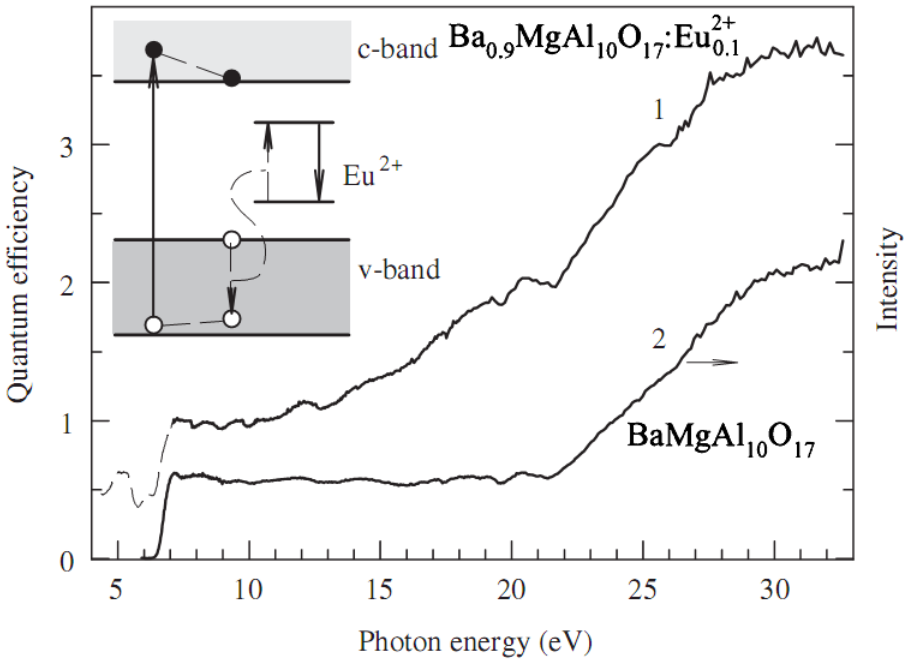

Figure 43. The quantum efficiency spectrum of the 2.72 eV emission of Eu^{2+} centers in penta-alumina BAM:Eu^{2+} (10%) at 295 K and the excitation spectrum for the 5.1 eV intrinsic emission in BAM at 8 K. The inset shows a simplified energy-band diagram of a BAM:Eu^{2+} phosphor: solid arrow lines indicate the absorption and emission of a photon, dashed arrow lines – the energy transfer by a hot hole to Eu^{2+} center due to the Auger process [48].

In an ordinary penta-alumina BAM:Eu^{2+} (10 mol %) phosphor, the efficiency of europium emission at the excitation by 7.8-9.0 eV photons at 295 K is QY ≈ 0.95 ± 0.05, i.e. the efficiency of nonradiative transitions is very low and the energy of almost each exciting photon is transformed into a blue emission (**Fig. 43**).

According to **Fig. 43,** in penta-alumina BAM:Eu^{2+} (10 mol %) the efficiency of impurity emission is QY ≅ 1 at $h\nu_{ex}$ = 7.8-10 eV and the value of QY starts to increase with a further rise of exciting photon energy ($h\nu_{ex}$), doubles in the range of 13-20 eV and continues increasing up to $h\nu_{ex}$ = 32 eV. Intrinsic UV emission dominates in the emission spectrum of BAM at 8 K and the drastic rise of the efficiency of this emission occurs only at $h\nu_{ex}$ > 20 eV, when an exciting photon is able to form two or more e–h pairs. In his recent work [49], A. Lushchik et al. showed that the rise of QY in BAM:Eu^{2+} (10 mol %) at $h\nu_{ex}$ > 13 eV is connected with the direct excitation of Eu^{2+} ions by the hot valence holes formed at the absorption of exciting photons. The energy excess (with respect to the top of the valence band) of a nonrelaxed (hot) hole is transferred to Eu^{2+} and an excited ion emits the first quantum of impurity luminescence. The recombination of a conduction electron with the relaxed valence hole near a Eu^{2+} center provides the second photon of europium emission. We have to remember, that industrial PDPs usually contain the mixture of two noble gases – Xe and Ne. The energy of neon resonance discharge emission is 16.7 eV, and as it can be seen from **Fig. 43**, such photons can create hot charge carriers. It is possible, that the direct excitation of several impurity ions by hot carriers causes the suppression of defect creation via hot e–h recombination, thus increasing the radiation resistance of materials ("luminescence protection") [48,50].

Final set of experiments was conducted to obtain the emission spectra (cathodoluminescence) for compounds № 59 – $Ba_{0.997}MgAl_{10}O_{17}:Eu_{0.003}$ and № 67 – $Ba_{0,95}MgAl_{14}O_{23}:Eu_{0,05}$. Objects were excited using an electron gun (6 keV, 30 nA / 1 μA per cm^2). Response of our objects to high energy electrons is presented in **Figs. 44** and **45**.

In **Fig. 44**, the main emission band is peaked at 2.82 eV, which corresponds to wavelength of 440 nm. This broad emission band is reported to be the $4f^6 5d^1 \rightarrow 4f^7$ transition in a Eu^{2+} ion substituted for a Ba^{2+} ion in the mirror planar between spinel blocks [51]. **Fig. 44** also demonstrates a partial transformation of Eu^{2+} into Eu^{3+}: a weak emission peak at 2.075 eV (597 nm) corresponds to trivalent europium (Eu^{3+}).

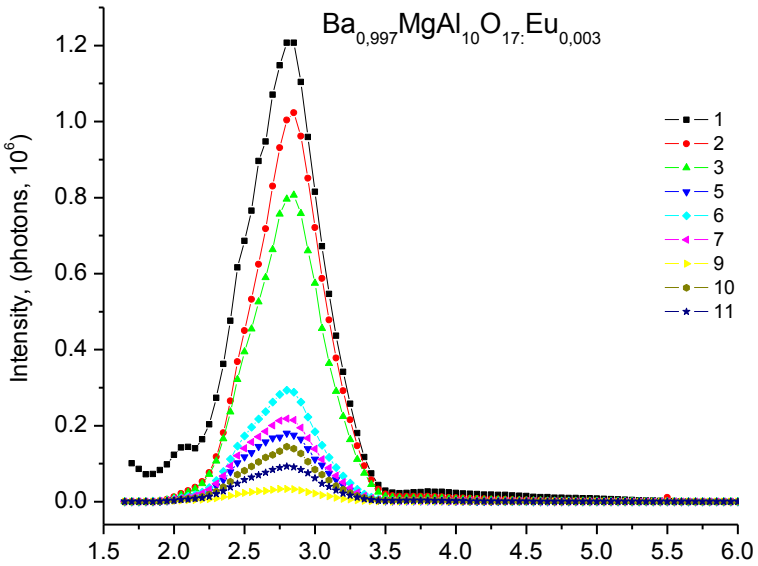

Figure 44. Emission spectra measured during the excitation of sample № 59(b) ($Ba_{0.997}MgAl_{10}O_{17}:Eu_{0.003}$) by 6 keV electrons (30 nA) at T = 295 K with 10 minute intervals between sequent measurements. Legend numbers depict order, in which spectra were obtained.

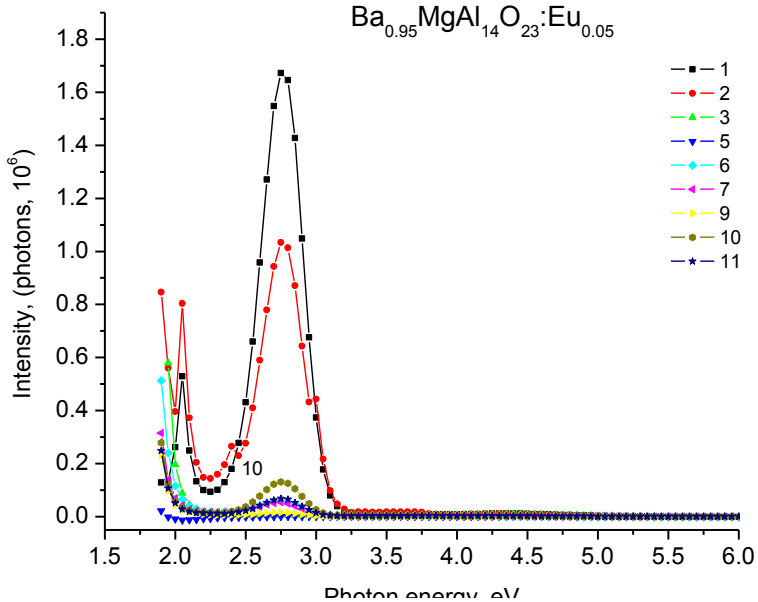

Figure 45. Emission spectra measured during the excitation of sample № 67 (b) ($Ba_{0,95}MgAl_{14}O_{23}:Eu_{0,05}$) by 6 keV electrons (30 nA) at T = 295 K with 10 minute intervals between sequent measurements. Legend numbers depict order, in which spectra were obtained.

In **Fig. 45**, the main emission band (2.75 eV, 451 nm), detected in septa-alumina BAM phosphor ($Ba_{0,95}MgAl_{14}O_{23}:Eu_{0,05}$), is related to the same $4f^6 5d^1 \rightarrow 4f^7$ transitions in Eu^{2+} Peak position coincides with that for a penta-alumina BAM phosphor ($Ba_{0.93}MgAl_{10}O_{17}:Eu_{0.07}$) [20]. Peak located at 1.9-2.2 eV is tentatively related to the emission of Eu^{3+}. It is important to mention, that at the beginning of irradiation, object emitted purple light.

Form **Figs. 44** and **45,** we can see how our objects of interest, $Ba_{0,95}MgAl_{14}O_{23}:Eu_{0,05}$ and $Ba_{0.997}MgAl_{10}O_{17}:Eu_{0.003}$, are affected by prolonged exposure to 6 keV electrons. Already after the second irradiation cycle, emission intensity decreased approximately by a factor of two and after the third, by ten times. Several complex emission peaks of minor intensity were registered as well. It should be mentioned, that there are several jumps of emission intensity decrease with radiation time. After irradiating objects and letting them to "cool down", peaks tend to rise at first, but then intensity decreases again. This can be explained by the fact, that samples tend to charge under the electron beam. The last circumstance causes the shift of the excitation spot on the phosphor surface (different regions are excited).

8. Summary

Degradation processes in $BaMgAl_{10}O_{17}:Eu^{2+}$ and $BaMgAl_{14}O_{23}:Eu^{2+}$

Master thesis of Semjon Galajev

Plasma display panels are a new technique for large-screen television sets and were the object of huge improvements during last decade. However, phosphors used tend to degrade, loosing quantum efficiency and stability. Processes of radiation aging of BAM phosphors are studied insufficiently. The analysis of the literature data on the degradation processes in barium magnesium aluminates connecter with both baking processes in the air (during PDP fabrication) and prolonged operation under irradiation (creating electrons and holes) has been performed. A partial oxidation of Eu^{2+} situated at the planes between spinel blocks as well as the harmful diffusion of europium ions from the phosphor occur at the spreading of $BaMgAl_{10}O_{17}:Eu^{2+}$ during the fabrication procedure.

In this work, synthesized Barium Magnesium Aluminate (BAM) with different Al_2O_3 and various Eu^{2+} content ($BaMgAl_{14}O_{23}:Eu^{2+}$), as well as some related compounds were subjected to several experimental methods: thermostimulated luminescence, excitation spectra by VUV-radiation, cathodoluminescent spectra.

Our experiments demonstrate that the irradiation of $BaMgAl_{10}O_{17}:Eu^{2+}$ and $BaMgAl_{14}O_{23}:Eu^{2+}$ (synthesized at the Institute of Tartu with our participation) by X-rays/an electron beam at room temperature causes the decrease of the efficiency of Eu^{2+}-luminescence. The similar suppression of impurity luminescence efficiency takes place under VUV irradiation in the region of host fundamental absorption (inside spinel blocks). It is shown that the efficiency of energy storage during X-irradiation (estimated via light sum of TSL) decreases with the rise of europium concentration. Such decrease is connected with the efficient energy transformation into beneficial fast impurity emission. Further investigation of "luminescent protection" against radiation damage in BAM phosphors by means of direct experimental methods lies ahead.

From obtained emission spectra, it was possible to demonstrate, that the synthesized compounds contain different phases, and that Eu^{2+} can be situated in different positions within the lattice. Possible presence of Eu^{3+} was noticed, which in turn explains the color

shift and proves oxidation of Eu^{2+} ions during synthesis. During cathodoluminescence experiments, decrease of blue light emission intensity and increase in red light emission intensity was observed.

It was pointed out, that the rise of QY in BAM:Eu^{2+} (10 mol %) at $h\nu_{ex} > 13$ eV (including the region of neon resonant discharge emission) is connected with the direct excitation of Eu^{2+} ions by the hot valence holes formed at the absorption of exciting photons. The energy excess of a nonrelaxed hole is transferred to Eu^{2+} and an excited ion emits the first quantum of impurity luminescence. The recombination of a conduction electron with the relaxed valence hole near a Eu^{2+} center provides the second photon of europium emission.

A comparative study of radiation damage in $BaMgAl_{10}O_{17}:Eu^{2+}$ and $BaMgAl_{14}O_{23}:Eu^{2+}$ (at present the latter is widely used in large-size PDP) has been shown that the efficiency of the energy transfer to Eu^{2+} centers by electron-hole pairs in $BaMgAl_{10}O_{17}:Eu^{2+}$ in close to unity in the region of resonant xenon discharge emission (8.43 eV) and QY > 1 at the excitation by resonant neon discharge emission (16.7 eV). However, there are favorable conditions for the diffusion of oxygen ions and following oxidation of Eu^{2+} centers in penta alumina BAM ($BaMgAl_{10}O_{17}$), where the structure of Ba-O planes with europium centers are rather far from the close-packed structure. Such diffusion can be stimulated by irradiation creating anion vacancies and oxygen interstitials.

The efficiency Eu^{2+}-emission excitation by 8.43 eV photons in $BaMgAl_{14}O_{23}:Eu^{2+}$ with more complicated structure is significantly lower (QY ≈ 0.6). However, one would expect that the diffusion (thermally or radiation-stimulated) of oxygen interstitials to Eu^{2+} centers (there is less empty space in Ba-O-planes) in this matrix be impeded. Unfortunately, the determination of detail structure of septa alumina BAM is not clear yet.

Proposed and synthesized compound – $BaMgAl_{14}O_{23}:Eu^{2+}$ – turned out to be more complicated than was expected. With every original piece of experimental data new challenges came to light. More thorough research on the protection against radiation induced degradation lies ahead.

9. Acknowledgements

The author is grateful to D.Sc. Professor Aleksandr Lushchik for competent supervision and years of teaching, to Academician Cheslav Lushchik for priceless advices and remarks, to Ph.D. Aarne Maaroos for introduction to practical synthesis, to Drs. Irina Kudryavtseva, Peeter Liblik and Evgeni Vassil'chenko for their time, experience and guidance during experiments. I am also very thankful to Külvi Noor, Ph.D. Fjodor Savikhin and my parents for endless support and help during the process of writing.

10. References

[1] B. Moine, G. Bizarri, "Why the quest of new rare earth doped phosphors deserves to go on," Optical Materials, **28**, 58–63, 2006

[2] J.P. Boeuf, Th. Callegari, P. Sabatier "Physics of a PDP Discharge Cell," in Conference Record of the Industry Applications Conference 2003. 38th IAS Annual Meeting, **1**, 69–73, 2003

[3] C.-H. Kim , I.-E. Kwon, C.-H. Park , Y.-J. Hwang , H.-S. Bae, B.-Y. Yu , C.-H. Pyun , G.-Y. Hong, "Phosphors for plasma display panels," Journal of Alloys and Compounds, **311**, 33–39, 2000

[4] J. P. Boeuf, "Plasma display panels: physics, recent developments and key issues," Journal of physics D: applied physics**, 36**, 53–79, 2003

[5] H.-C. Lu, H.-K. Chen, T.-Y. Tseng, W.-L. Kuo, M.S. Alam, B.-Mi. Cheng, "Photoluminescence of phosphors for PDP with VUV excitation," Journal of Electron Spectroscopy and Related Phenomena, **144-147**, 983–985, 2005

[6] A. Bogaerts, E. Neyts , R. Gijbels , J. van der Mullen, "Gas discharge plasmas and their applications," Spectrochimica Acta, Part B **57**, 609–658, 2002

[7] C. Ronda, *Luminescence: From Theory to Applications* (Wiley-VCH, 2007).

[8] R.C. Ropp, *Luminescence and the Solid state* (Elsevier Science, 2nd edition, 2004).

[9] S. Shionoya, W.M. Yen, H. Yamamoto, *Phosphor Handbook* (CRC Press, 2nd edition, 2006).

[10] S. Shionoya, W.M. Yen, H. Yamamoto, *Fundamentals of Phosphors* (CRC Press, 2007).

[11] P. Yang, G.-Q. Yao, J.-H. Lin, "Energy transfer and photoluminescence of $BaMgAl_{10}O_{17}$ co-doped with Eu^{2+} and Mn^{2+}," Optical Materials, **26**, 327–331, 2004

[12] T. Jüstel, H. Bechtel, W. Mayr, D. U. Wiechert, "Blue emitting $BaMgAl_{10}O_{17}$:Eu with a blue body color," Journal of Luminescence, **104**, 137–143, 2003

[13] V. Ramesh Kumar, K.V. Narasimhulu, N.O. Gopal, J.L. Rao, R.P.S. Chakradhar, "EPR and optical investigations of Eu^{2+}-doped BaFCl phosphor," Physica B, **348**, 446–453, 2004

[14] L.L Chase, "Microwave-optical double resonance of the metastable $4f^6 5d$ level of Eu^{2+} in the fluorite lattices," Physical Review B, **2**, 1970

[15] A. Daud, T. Kunimoto, R. Yoshimatsu, K. Ohmi, S. Tanaka and H. Kobayashi, "Blue and red emitting Eu activated $CaMgSi_2O_6$ VUV phosphors," in ICSE2000 Proceedings, pp. 128-130, Nov. 2000

[16] G. Blasse, "On the nature of the Eu^{2+} luminescence," Physica Status Solidi B, **55**, 131-134, 1973

[17] A. Suchocki, S.W. Biernacki, M. Grinberg, "Nephelauxetic effect in high-pressure luminescence of transition-metal ion dopants," Journal of Luminescence, **125**, 266–270, 2007

[18] S. Oshio, T. Matsuoka, S. Tanaka, H. Kobayashi, "Mechanism of luminance decrease in $BaMgAl_{10}O_{17}:Eu^{2+}$ phosphor by oxidation," Journal of The Electrochemical Society, **145**, Issue 11, 3903-3907, 1998

[19] Z. H. Zhanga, Y. H. Wanga, X. X. Li, Y. K. Dua, W. J. Liu, "Photoluminescence degradation and color shift studies of annealed $BaMgAl_{10}O_{17}:Eu^{2+}$ phosphor," Journal of Luminescence, **122–123**, 1003–1005, 2007

[20] G. Bizarri, B. Moine, "On $BaMgAl_{10}O_{17}:Eu^{2+}$ phosphor degradation mechanism: thermal treatment effects," Journal of Luminescence, **113**, 199–213, 2005

[21] K. Yokota, S.-X. Zhang, K. Kimura, A. Sakamoto, "Eu^{2+}-activated barium magnesium aluminate phosphor for plasma displays – Phase relation and mechanism of thermal degradation," Journal of Luminescence, **92**, 223–227, 2001

[22] S. Zhanga, T. Konoa, A. Itoa, T. Yasakaa, H. Uchiike, "Degradation mechanisms of the blue-emitting phosphor $BaMgAl_{10}O_{17}:Eu^{2+}$ under baking and VUV-irradiating treatments," Journal of Luminescence, **106**, 39–46, 2004

[23] P. Dorenbos, "Energy of the first $4f^7 \rightarrow 4f^6 5d$ transition of Eu^{2+} in inorganic compounds," Journal of Luminescence, **104**, 239–260, 2003

[24] K.A. Gschneidner Jr., J.-C.G. Bünzli, V.K. Pecharsky, *Handbook on the Physics and Chemistry of Rare Earths* (Elsevier B.V., Vol. 37, 2007).

[25] M. Stephan, P.C. Schmidt, K.C. Mishara, M. Raukas, A. Ellens, P. Boolchand, "Investigations of nuclear quadrupole interaction in $BaMgAl_{10}O_{17}Eu^{+2}$," Zeitschrift für Physicalische Chemie, **215**, 11, 1397-1411, 2005

[26] H. Toyoshimaa, S. Watanabe, K. Ogasawara, H. Yoshida, "First-principles calculations of 4f–5d optical absorption spectra in $BaMgAl_{10}O_{17}$:Eu," Journal of Luminescence, **122-123**, 104-106, 2007

[27] B. Moine , G. Bizarri, "Degradation mechanism of phosphors by vacuum ultraviolet excitation," Optical Materials, **28**, 587–591, 2006

[28] G. Bizarri, B. Moine, "On the role of traps in the $BaMgAl_{10}O_{17}:Eu^{2+}$ fluorescence mechanisms," Journal of Luminescence, **115**, 53–61, 2005

[29] W. Lehmann, "Phosphor deterioration in fluorescent lamps," Journal of The Electrochemical Society, 130, Issue 2, 426-431, 1983

[30] K. Hayashi, M. Watanabe, M. Terai, K. Arai, K. Ichinomiya, "The deterioration of blue phosphor for fluorescent lamps," Journal of Light and Visual Environment, **25**, 79-81, 2001

[31] B. Dawson, M. Ferguson, G. Marking, A. L. Diaz, "Mechanisms of VUV Damage in $BaMgAl_{10}O_{17}:Eu^{2+}$," Chemistry Of Materials, **16**, 5311-5317, 2004

[32] K.-B. Kim, K.-W. Koo, T.-Y. Cho, H.-G. Chun, "Effect of heat treatment on photoluminescence behavior of $BaMgAl_{10}O_{17}:Eu^{2+}$ phosphors," Materials Chemistry and Physics, **80**, 682–689, 2003

[33] P. Yang, G.-Q. Yao, J.-H. Lin, "Energy transfer and photoluminescence of $BaMgAl_{10}O_{17}$ co-doped with Eu^{2+} and Mn^{2+}," Optical Materials, **26**, 327–331, 2004

[34] P. Dorenbos, "Thermal quenching of Eu^{2+} 5d–4f luminescence in inorganic compounds," Journal of Physics: Condensed Matter, **17**, 8103–8111, 2005

[35] U. Vater, G. Künzler, W. Tews, "Quenching problems in inorganic luminescent materials," Journal of Fluorescence, **4**, 1, 79-82, 1994

[36] W. M. Yen, M. J. Weber, *Inorganic Phosphors: Compositions, Preparation and Optical Properties* (CRC Press, 1st edition, 2004).

[37] K.J. Thomsen, L. Botter-Jensen, P.M. Denbya, P. Moskab, A.S. Murray, "Developments in luminescence measurement techniques," Radiation Measurements, **41,** 768–773, 2006

[38] M. A. Linne, *Spectroscopic Measurement: An Introduction to the Fundamentals* (Academic Press, 1st edition, 2002).

[39] D. R. Vij, *Handbook of Applied Solid State Spectroscopy* (Springer Science, 2006).

[40] C. Furetta, *Handbook of Thermoluminescence* (World Scientific Publishing Company, 2003).

[41] S.W.S. McKeever, *Thermoluminescence of Solids* (Cambridge University Press, 1988).

[42] A. Lushchik, M. Kirm, A. Kotlov, P. Liblik, Ch. Lushchik, A. Maaroos, V. Nagirnyi, T. Savikhina, G. Zimmerer, "Intrinsic and impurity luminescence and multiplication of excitations in complex oxides," Journal of Luminescence, **102–103**, 38–43, 2003

[43] A. Lushchik, F. Savikhin, I. Tokbergenov, "Electron and hole intraband luminescence in complex metal oxides," Journal of Luminescence, **102–103**, 44–47, 2003

[44] R. T. Ellickson, "Light sum of phosphors under thermal and infra-red stimulation," Journal of the Optical Society of America, **36**, 5, 254–249,1946

[45] Ф.А. Савихин, "Линейные и сверхлинейные процессы при термостимулированной люминисценции кристаллофосфоров при фото-, α- и γ–возбуждении", Диссертиация на соискание ученой степени кандидата физико-матемических наук, Тарту 1972.

[46] S. Zhang, "Vacuum-Ultraviolet/Visible Conversion Phosphors for Plasma Display Panels," IEEE Transactions on Plasma Science, **34**, 2, 1–11, 2006

[47] B. Howea, A. L. Diaz, "Characterization of host-lattice emission and energy transfer in $BaMgAl_{10}O_{17}Eu^{2+}$," Journal of Luminescence, **109**, 51–59, 2004

[48] A. Lushchik, E. Feldbach, S. Galajev, T. Kärner, P. Liblik, Ch. Lushchik, A. Maaroos, V. Nagirnyi, E. Vasil'chenko, "Some aspects of radiation resistance of wide-gap metal oxides," Radiation Measurements, **42**, 4-5, 792–797, 2007

[49] A. Lushchik, Ch. Lushchik, E. Feldbach, I. Kudryavtseva, P. Liblik, A. Maaroos, V. Nagirnyi, F. Savikhin, E. Vasil'chenko "Photon multiplication in wide-gap BAM and SAM aluminates," in *Proceedings of the SPIE*, Rosental, Arnold. Ed (Optical Materials and Applications, **5946**, 61–72, 2005)

[50] A. Lushchik, Ch. Lushchik, M. Kirm, V. Nagirnyi, F. Savikhin, E. Vasil'chenko, "Defect creation caused by the decay of cation excitons and hot electron–hole recombination in wide-gap dielectrics," Nuclear Instruments and Methods in Physics Research B, **250** , 330–336, 2006

[51] M. Peng, J. Qiu, L. Yang, C. Zhao, "Observation of $Eu^{3+} \rightarrow Eu^{2+}$ in barium hexa-aluminates with β' or β-alumina structures prepared in air," Optical Materials, **27**, 591–595, 2004

11. Kokkuvõte

Lagunemisprotsessid $BaMgAl_{10}O_{17}:Eu^{2+}$ ja $BaMgAl_{14}O_{23}:Eu^{2+}$ sees

Magistritöö, Semjon Galajev

Plasma lamekuvarid, mis on uus tehnoloogia laia diagonaaliga ekraanide tootmiseks, olid eelmise kümnendi jooksul põhjaliku täiustamise objektiks. Ometigi nende oluline puudus on see, et spektraaltransformaatorid (fosfoorid) kipuvad lagunema, kaotades sellega kvantsaagist ja stabiilsust. Kiiritusest põhjustatud lagunemisprotsessid BAM fosfoorides vajavad veel uurimist. Kirjanduse analüüs näitas, et lagunemisprotsessid baarium-magneesium aluminaatides toimuvad nii paneeli valmistamise ajal (paagutamine õhus) kui ka pikaajalise töökoormuse (kiirituse all elektronide ja aukude moodustumine) vältel. Kahevalentse euroopiumi, mis asub spinelli plokkide vahelistel tasanditel, osaline oksüdeerimine ning euroopium ioonide defundeerimine toimub $BaMgAl_{10}O_{17}:Eu^{2+}$ paigladmaisel tootmisprotsessis.

Antud töös olid sünteesitud BAM fosfoorid erineva Al_2O_3 sisaldusega ning erineva Eu^{2+} sisaldusega. Saadud ühendi valem pidi olema $BaMgAl_{14}O_{23}:Eu^{2+}$. Eksperimentides olid rakendatud järgmised meetodid: termostimuleeritud luminestsents, ergastus spektrid VUV-kiiritusega ning katoodluminestsents.

Meie eksperimendid näitavad, et kiiritades $BaMgAl_{10}O_{17}:Eu^{2+}$ ja Tartu Ülikooli Füüsika Instituudis sünteesitud $BaMgAl_{14}O_{23}:Eu^{2+}$ röntgenkiirtega ja elektronidega toatemperatuuril – euroopiumi tsentrite luminestsents väheneb. Sarnane lisanditsentrite luminestsentsi supressioon toimub ka VUV kiiritamisel (spinelli plokis, põhiaine põhineeldumise piirkonnas). Näidatud on, et energia salvestuse efektiivsus röntgenkiirtega kiiritamisel väheneb, kui lisandi kontsentratsioon tõuseb (hindamine TSL valgussumma baasil). Selline vähenemine on seotud energia efektiivse transformatsiooniga kasulikuks lisanditsentri kiiremissiooniks. Põhjalikum eksperimentaalne uurimistöö, kuidas kaitsta BAM fosfoore lagunemise eest kiiritusel, kasutades „luminestsentskaitset“, on veel ees.

Saadud kiirgusspektreid võrreldes oli võimalik näidata, et sünteesitud ühendid sisaldavad erinevaid faase ja et Eu^{2+} võib asuda kristallvõres erinevates positsioonides. Eksperimendi käigus oli võimalik märgata Eu^{3+} tõenäolist kohalolekut, mis võimaldab seletada nii

värvinihet kui ka tõestada, et Eu^{2+} ioonid oksüdeeruvad sünteesi käigus. Katoodluminestsentsi eksperimentide vältel oli näha, kuidas sinise valguse kiirgamisintensiivsus väheneb ja kuidas tekib juurde punane kiirgus.

Eksperimentide käigus toodi välja, et kvantsaagise tõus BAM:Eu^{2+} (10 mol %) fosfooris, kui seda kiiritati $h\nu_{ex} > 13$ eV (siia kuulub ka neooni resonants-gaaslahenduse kiirgus), on seotud Eu^{2+} ioonide otsese ergastamisega kuumade aukudega, mis tekivad ergastavate footonite neelamisel. Relakseerumata aukude liigne energia antakse üle Eu^{2+} ioonidele ja ergastatud ioon kiirgab seejärel esimese lisandikiirguse kvandi. Juhtivuselektroni ja relakseerunud augu rekombinatsiooni protsess, mis toimub Eu^{2+} tsentrite kõrval, annab teise Eu^{2+} kiirguse footoni.

Kiirguskahjustuse võrdlev uuring $BaMgAl_{10}O_{17}:Eu^{2+}$ ja $BaMgAl_{14}O_{23}:Eu^{2+}$ fosfoorides (viimast kasutatakse praegu laialt paneelide tootmises) näitas, et energia ülekandmise efektiivsus Eu^{2+} tsentritele $BaMgAl_{10}O_{17}:Eu^{2+}$ fosfooris elektron-auk paaride poolt, on väga lähedane ühele (ksenoon resonants-gaasilahenduse kiirguse (8.43 eV) puhul). Neoon resonants-gaasilahenduse kiirguse (16.7 eV) puhul on kvantsaagis suurem kui üks. Penta-alumina BAM fosfooris, kus Ba-O tasandite struktuur koos Eu^{2+} ioonidega on pigem suhteliselt kauge tihedalt pakitud struktuurist, esinevad soodsad tingimused hapniku ioonide defundeerimiseks. Sellest tuleneb Eu^{2+} tsentrite oksüdeerimine. Sellist difusiooni võib stimuleerida kiirgusega, tekitades sellega anioonvakantse ja hapniku interstitsiaale.

Kui $BaMgAl_{14}O_{23}:Eu^{2+}$ on ergastatud 8.43 eV footonitega, siis Eu^{2+} kiirguse efektiivsus on oluliselt madalam kui $BaMgAl_{10}O_{17}:Eu^{2+}$ (kvantsaagis ≈ 0.6), kuigi võis oodata, et termo – või kiirituse stimuleeritud hapniku interstitsiaalide difusioon Eu^{2+} tsentrite juurde (seal on vähem vaba ruumi Ba-O tasandites) selles struktuuris on raskendatud. Senini $BaMgAl_{14}O_{23}:Eu^{2+}$ struktuur ei ole veel selgeks tehtud.

Pakutud ja sünteesitud ühend - $BaMgAl_{14}O_{23}:Eu^{2+}$ - osutus keerulisemaks, kui oli alguses võimalik arvata. Iga eksperimentides saadud uue andmekogusega, ilmusid järjekordsed probleemid. Põhjalikumad uuringud, kuidas materjale kiirguse eest kaitsta, on veel ees.